



POLITECNICO DI TORINO

Corso di Laurea in NANOTECHNOLOGIES FOR ICT

Master Degree Thesis

**Modification of nanostructured  
tin oxide-based catalysts for  
 $CO_2$  valorization**

**Supervisors**

Prof. PIRRI CANDIDO

Dr. BEJTKA KATARZYNA

Dr. CHIODONI ANGELICA

**Candidate**

NICOLÓ BRUNO DOMENICO MONTI

ACADEMIC YEAR 2018-2019

# Acknowledgements

I would love to thank all the people who allowed and helped me in completing my masted degree course and my thesis work.

I would like to thank the IIT Center for Sustainable Future Technologies that allowed me to participate and study for this topic which I have been interested about for many years. I am thankful to Prof. Pirri Fabrizio and Dr. Chiodoni Angelica who allowed me to participate in this research, and also to Dr. Katarzyna Bejtka, who introduced me into the research field. I personally thank Dr. Juqin Zeng and Dr. Adriano Sacco that gave me support during electrochemical experiments, Umberto Savino who gave me useful advice, and also: Alberto, Amin, Daniele, Denis, Giulio, Stefania and all the other IIT's staff member.

# Contents

<b>1</b>	<b>Introduction</b>	<b>5</b>
1.1	Greenhouse causes and effects . . . . .	5
1.2	World primary energy consumption . . . . .	7
1.3	Strategies for reduction of $CO_2$ generation . . . . .	9
1.4	Electrochemical $CO_2$ reduction reaction . . . . .	9
1.5	Tin oxide based catalysts for $CO_2RR$ . . . . .	11
1.6	Goal and organization of the thesis . . . . .	11
<b>2</b>	<b>Introduction to used technologies</b>	<b>13</b>
2.1	Anodic Oxidation . . . . .	13
2.2	Doping . . . . .	22
2.3	Annealing . . . . .	25
2.4	Field Emission Scanning Electron Microscopy (FESEM) . . . . .	26
	2.4.1 Energy-dispersive X-Ray (EDX) . . . . .	29
2.5	X-Ray Diffraction (XRD) . . . . .	29
<b>3</b>	<b>Introduction to electrocatalysis</b>	<b>31</b>
3.1	Electrochemical reduction of carbon dioxide $CO_2RR$ . . . . .	31
3.2	Electrochemical set-up . . . . .	37
3.3	Cycling Voltammetry . . . . .	42
3.4	Chromatographic analysis . . . . .	44
	3.4.1 High Performance Liquid Analysis (HPLC) . . . . .	44
	3.4.2 Gas Chromatography (GC) . . . . .	46
<b>4</b>	<b>Results and discussion on <math>SnO_2</math> based electrode</b>	<b>47</b>
4.1	$SnO_2$ synthesis and characterization . . . . .	47
4.2	Preparation of Tin oxide catalyst . . . . .	50
	4.2.1 Tin oxide removal from the metallic tin substrate . . . . .	50
	4.2.2 Annealing . . . . .	54

4.3	Electrodes preparation . . . . .	54
4.4	Electrochemical characterization . . . . .	56
4.5	Conclusions . . . . .	58
<b>5</b>	<b>Results and discussion on modified <math>SnO_2</math> based electrode</b>	<b>61</b>
5.1	$SnO_2$ doping and characterization . . . . .	62
5.1.1	EDX analysis . . . . .	64
5.2	Electrodes preparation and characterization . . . . .	66
5.2.1	XRD analysis . . . . .	66
5.3	Electrochemical characterization . . . . .	67
5.3.1	Cycling voltammetry . . . . .	67
5.3.2	Chronoamperometric Measurements . . . . .	69
5.4	Tested electrode characterization . . . . .	75
5.5	Discussion on electrodes results . . . . .	76
<b>6</b>	<b>Conclusions and perspectives</b>	<b>79</b>
	<b>Bibliography</b>	<b>83</b>

# Chapter 1

## Introduction

“The vast preponderance of evidence, based on years of research conducted by a wide array of different investigators at many institutions, clearly indicates that global climate change is real, it is caused largely by human activities, and the need to take action is urgent.” [1]

said Alan I. Leshner, chief executive officer of American Association for the Advancement of Science (AAAS) and executive publisher of the journal *Science*, in the letter (AAAS Reaffirms Statements on Climate Change and Integrity) sent the 21 October 2009 to the US Senate. It was signed by 18 leading organisations leaders. Concrete actions were taken by the nations, specifically by signing different agreements. The more recent is the Paris Agreement negotiated during the XXI Conference Of the Parties of the United Nations Framework Convention on Climate Change (UNFCCC), which entered into effect starting from the 4 November 2016. Nowadays, it has been ratified by 186 states, UNFCCC members.

### 1.1 Greenhouse causes and effects

The climate change is causing a wide range of impacts that at some point, will affect every human on Earth in increasingly severe ways. Many changes in the nature, including the shift of plants and animals species, with the consequent extinction risk for some of them, and other changes in vegetation, like the fact that trees blossom sooner, observed in recent years, are now attributed to the climate change. At the same time, the mass media reported other events such as the glacial ice melting and sea level rising [2]. In the past 100 years, the sea level has been increased of almost 18cm; some predictions theorize a

further level increase from 30cm up to 122cm by 2100 [2]. The above listed and other climate changes are caused by the global temperature variation. The Intergovernmental Panel on Climate Change predicts a temperature rise of 3.9°C up to 12.2°C over the next century [2]. Starting from the industrial revolution, global temperature has increased of about 0.8°C even if the solar irradiance has been remained almost constant [3]. The temperature raising is related to the greenhouse effect. It is the consequence of the variation of some gas concentration in the atmosphere, especially:  $CO_2$ ,  $H_2O$ ,  $CH_4$  that trap the heat radiating from the Earth towards space. This is caused by the gas absorption spectrum, which is active in the infrared wavelengths. Water ( $H_2O$ ) is the most abundant of these, and it is generated mainly by evaporation. It acts as a feedback system because a temperature rise increases its concentration in the atmosphere that further promotes the water evaporation. The temperature increase promotes the oceans heating that decreases their carbon dioxide concentration, which in turn is released into the atmosphere, further contributing to the greenhouse effect [3]. The methane is produced by bacteria digestion during the decomposition of dead organisms [3]. Methane ( $CH_4$ ) has a lifetime in the atmosphere of almost 8 years. Instead, carbon dioxide ( $CO_2$ ), which historically was released naturally by volcano eruptions and by living organism respiration, since the industrial era has been released in a huge quantity because of the fossil fuel combustion. It is a stable and nonreactive molecule, therefore it has a very long lifetime. In nature, only the chlorophyll photosynthesis can fix it reducing its quantity in the air, transforming it into a sugar molecule [3]. Its concentration in the atmosphere during the geological eras reached a value of 300 ppm, but the industrial revolution drastically increased it. Its concentration given by human activity is rising every day, Figure 1.1 shows an estimation of  $CO_2$  levels in the past hundreds of thousands of years. In October 2019 it reached 412 ppm, measured in Mauna Loa Observatory, Hawaii [4].

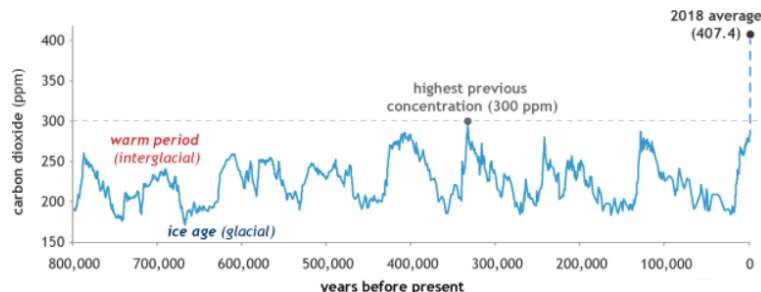


Figure 1.1:  $CO_2$  during the past 800 000 years [5].

## 1.2 World primary energy consumption

The human need of energy is strictly related to the carbon dioxide emission, because the technologies to produce energy are mainly based on combustion. Therefore to provide an idea of the energy demand and  $CO_2$  emission for example during the year 2015, estimated by International Energy Agency. The world primary energy consumption was of 13 647 Mtoe (Million Tonnes of Oil Equivalent). The primary energy sources were the fossil fuels (coal, natural gas and oil). The energy production of these sources requires their combustion, but also biofuels and waste need to be burnt to produce energy. Figure 1.2a shows the percentage distribution of the different energy sources. This shows that 91.1% of energy sources in 2015 released carbon dioxide and other pollutants in the atmosphere because of their combustion. In 2015 the carbon dioxide released from fuel combustion was 32 294Mt (Metric tons), Figure 1.2b shows its distribution by the production source.

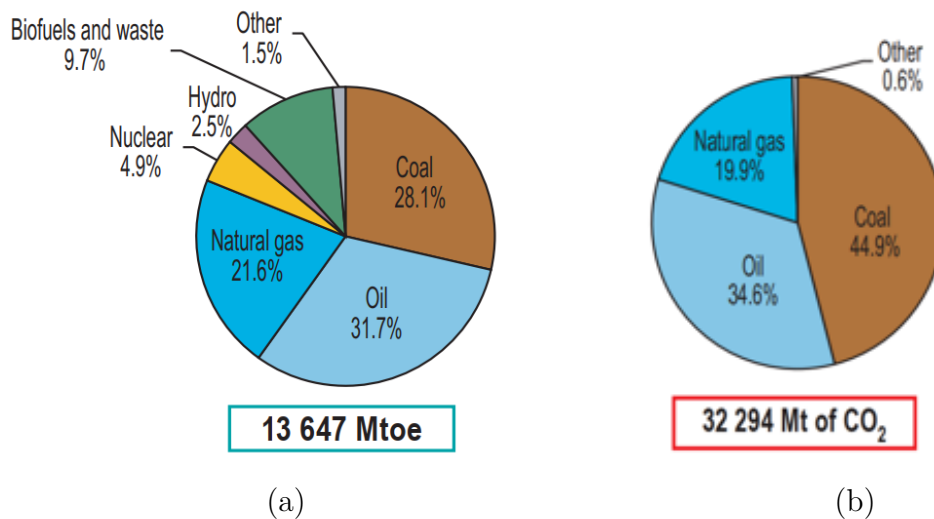


Figure 1.2: (a) World primary energy sources in 2015 [6], (b)  $CO_2$  sources [6].

The energy demand continuously increases, and one of the reasons is the increase in global population. Today there are 7.4 billion of people, and the predictions estimate 9 billions of people in 2040 [7]. To provide good welfare to everyone, the energy consumption will have to grow. Also the rapid industrialization of south-east Asia will increase the need of energy. The predictions estimate that China will consume for cooling in 2040 the same amount of whole energy used by Japan in 2015 [7].

The energy demand and related carbon dioxide emission might have a different distribution in 2040 [8]. The *BP Energy Outlook: 2019 edition* predict four possible scenarios including: More Energy (ME) characterized by a huge increase of energy consumed; Evolving Transition (ET) where the energy demand should not consume more fossil fuels; Less Globalization (LG) predicts a smaller energy consumption and Rapid Transition (RT) scenario theorize a controlled increase of energy consumption and a big improvement of the renewable energy sources and a reduction of emitted carbon dioxide. The graph 1.3 shows the predicted change in  $CO_2$  emission as a function of time, according to those different scenarios.

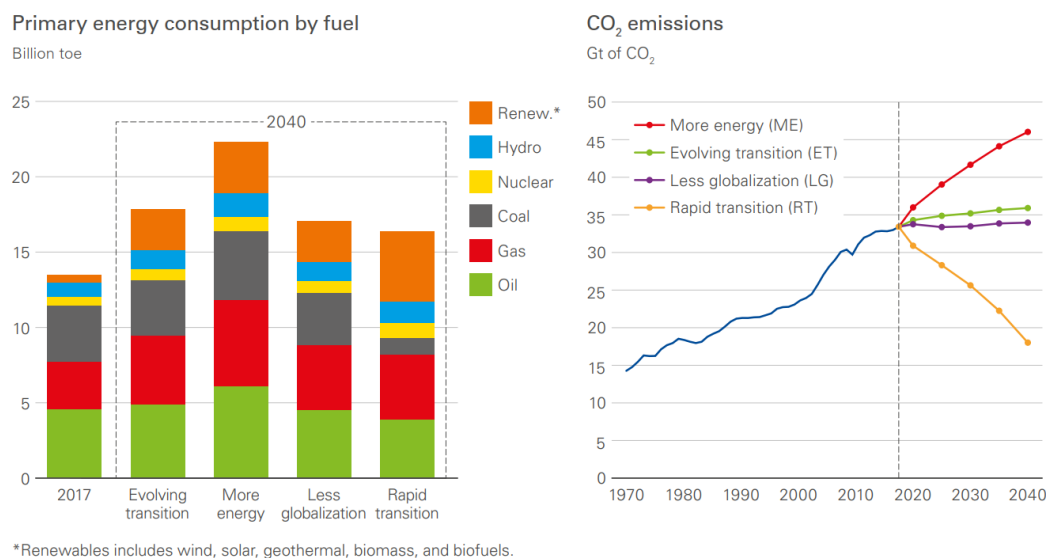


Figure 1.3: Energy consumption prediction by fuel (left) and consequent  $CO_2$  emission in 2040 (right) [8].

Which one will be correct, will be determined by the choices that nations will make in the next years. This includes fulfilment and the positive overcoming of the Paris climate agreement expectations, ratified during the XXI UNFCCC.

## 1.3 Strategies for reduction of $CO_2$ generation

The Governments authorities, through the actuation of specific policies, can ensure the reducing carbon dioxide emissions. In addition to this, the future technological development might reduce the carbon dioxide generation thanks to a rapid improvement of the renewable energy sources. It will be possible to increase their exploitation through their cost reduction, and the increased of batteries performance.

A parallel action to decrease the carbon dioxide released in the atmosphere is the Carbon-Capture-Utilization-and-Storage (CCUS). It is an emission reducing technology, it captures the emitted  $CO_2$  from an industrial process or fuel combustion, then store it in geological formation or convert in reusable products [9]. According to the current technologies and the sources market values, the estimations foresee that CCUS technology exploitation might reach 10% of installed power generation capacity in 2040 [10].

The most promising sector is to convert the  $CO_2$  generated by power plants or chemical facility. The process is divided into different steps according to Figure 1.4.

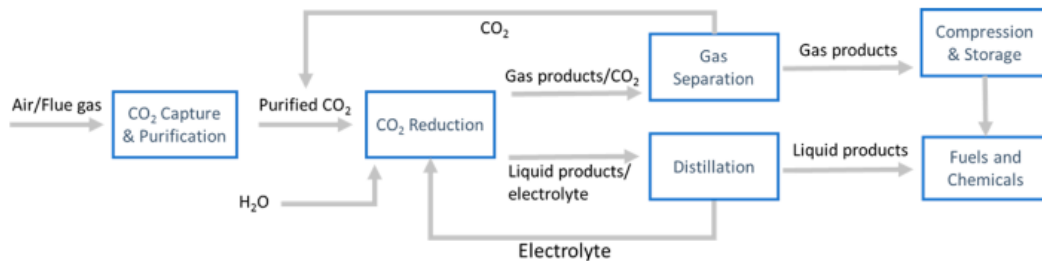


Figure 1.4: Schematic of general  $CO_2$  electrolysis process [11]

It includes four steps:  $CO_2$  capture, purification, reduction and use. The most promising technology to reduce the carbon dioxide concentration are the renewable energy sources exploitation and the carbon dioxide reduction process through electrochemical conversion.

## 1.4 Electrochemical $CO_2$ reduction reaction

$CO_2$  electrochemical reduction is a good way to reduce its concentration in the atmosphere and obtain value-added products. The energy needed

for the process can be supplied by renewable energy sources. This reaction might generate carbon monoxide, formic acid, methane, n-propanol and others according to the number of exchanged electrons. The most promising compounds for a rapid industrial application of this technology are carbon monoxide ( $CO$ ) and formic acid ( $HCOOH$ ). This is because they require smaller capital and operating cost, which is strictly related to smaller electrical current needs per kilogram of product [11].

Carbon monoxide is used, coupled with hydrogen, as syngas. It has many application as intermediate for the synthetic natural gas production [12], or to produce methanol [13], but also for electricity generation [14]. The formic acid global consumption is 0.6 Mtoe [11], and its demand is also rising because its applications are increasing.  $HCOOH$  is used in agriculture and manufacturing as a benign organic acid. Its salts are used as deicing agents for airports. An interesting emerging application for formic acid is as hydrogen carrier and as a fuel for fuel cells [15]. It has a high volumetric density of 53g  $H_2$  per litre with a corresponding higher volumetric energy density (2086Wh/L) compared to the  $H_2$  fuel [16].  $CO$  and  $HCOOH$  are usually produced from fossil fuels, therefore the possibilities to obtain them from waste material like  $CO_2$  will be an appealing goal. According to Matthew Jouny and co-workers predictions, focused on the end of life Net Present Value (NPV), it is possible to obtain positive values for  $CO$  and  $HCOOH$  (as Figure 1.5 shows).

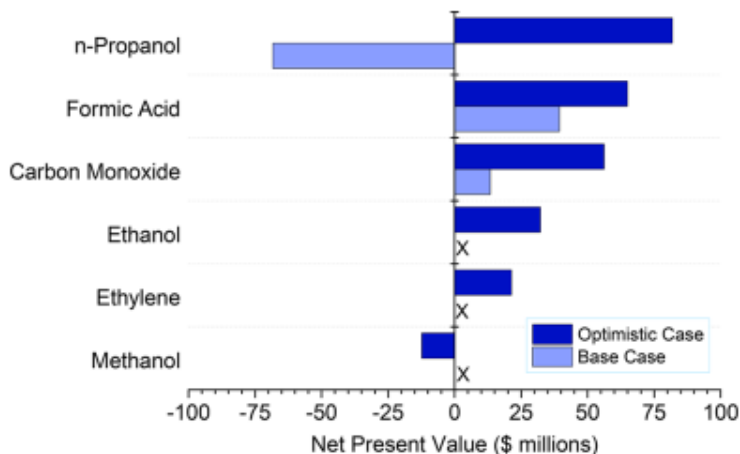


Figure 1.5: End-of-life NPV values for the production of various chemicals through electrochemical  $CO_2$  reduction [11].

The set-up devoted to the formic acid and carbon monoxide production are

the cheapest and more appealing [11]. Therefore among many products that can be obtained, which depend on the catalyst characteristics, reaction conditions and electrolyte, the  $CO_2$  reduction reaction ( $CO_2RR$ ) to  $CO$  and  $HCOOH$  is up to now the most economically viable processes that can be competitive to the conventional production routes [11].

## 1.5 Tin oxide based catalysts for $CO_2RR$

The  $CO_2RR$  requires a catalyst, usually supported on a conductive substrate. The optimal catalyst should generate at the same time a good selectivity towards the desired products, the highest possible conversion efficiency and the minimum energy supply. Different transition metals and metal oxides have been tested as  $CO_2RR$  catalysts [17]. The competitive product of  $CO_2RR$  is the Hydrogen Evolution Reaction (HER). Other metals are more sensible to the formate production such as tin and indium; until now only copper might produce hydrocarbons.

$Sn/SnO_2$ -based catalysts are very interesting because their products are  $CO$  and  $HCOOH$ . Therefore it might be a good candidate for the transition of the  $CO_2RR$  up to the industrial scale. In addition tin is eco-friendly material, inexpensive and earth-abundant. In literature  $Sn/SnO_2$ -based catalysts have been produced with different forms and shapes, including:  $Sn/SnO_2$  porous hollow fiber [18],  $SnO_2$  nanosheet/Carbon cloth [19],  $SnO_x$  nanoparticles [20], electro-deposited Sn [21], Sn particles [22],  $SnO_2$  nanopowder [23],  $SnO_2$ /graphene [24], Sn dendrite [25], Sn-Nafion [26],  $SnO_2$  porous NWs [27]. They were produced with different synthesis routes: hydro-thermal synthesis [24], electrodeposition [25], solvo-plasma technique [18] and anodic oxidation [28]. This thesis work is focused on the anodization process to obtain tin oxide.

## 1.6 Goal and organization of the thesis

In this thesis  $SnO_2$  catalyst, obtained through anodic oxidation, which is simple, low cost, scalable, high yield and effective strategy to obtain a nanostructured material, is studied for  $CO_2RR$ . The goal is to improve its electrochemical performances by introducing dopant elements, according to the theoretical calculations proposed in the literature [29]. Authors demonstrated that the insertion of the dopant atoms, placed in the position near to adsorbate binding sites, affects the adsorbate binding energy and results in

improved catalytic properties and reduced overpotential. The methods and technological approaches used in this work to prepare the undoped catalyst and the related electrodes, follow up from previously optimized procedures. The preparation of the doped catalyst is developed and optimized within this thesis work.

The thesis is organized as follows: Chapter 2 is devoted to the technologies used to create, dope and characterize tin oxide. Chapter 3 focuses on  $CO_2RR$ , the used setup and the analysis of the obtained products. Chapter 4 describes the material preparation and characterisation; electrode fabrication procedures and electrochemical tests; and at last some improvements introduced to the electrode fabrication procedure in order to obtain better performing and reproducible electrodes. Chapter 5 relates to the doped tin oxide catalyst, to the material preparation and characterisation; to the preparation of the electrodes and characterisation of their performances. It will be demonstrated that the produced doped  $SnO_2$ -based electrodes result in improved catalytic properties, including  $HCOOH$  production. Finally, in the last chapter, some conclusions are drawn.

Good reading!

# Chapter 2

## Introduction to used technologies

### 2.1 Anodic Oxidation

It is an electrochemical process usually used to increase the oxide thickness, to protect the material from corrosion and change its surface properties. In this last case, the goal is to modify the surface morphology and its composition. It is also used to obtain porous structures by oxidizing *Al*, *Ti*, *Sn* and some other metals. The most widely studied are  $Al_2O_3$  and  $TiO_2$ . In recent years  $SnO_x$  was studied for optical applications [30] carbon dioxide reduction [28] and others. The synthesis is simple, low-cost and straight-forward. The charge transfer dominates the reaction process.

A schematic illustration of the set up is shown in Figure 2.1.

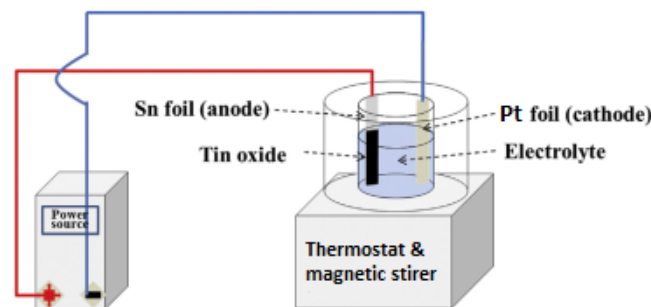
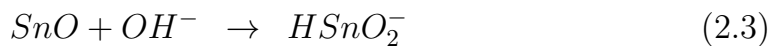
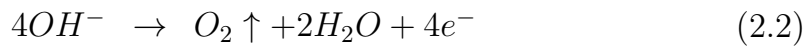
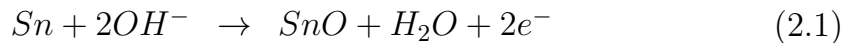


Figure 2.1: Schematic diagram of anodic oxidation system [31].

It is composed of a cell, two electrodes, an electrolyte and a power supply.

The cell should be filled with acid or basic solution. It has two tasks: to increase the charge transfer, providing a higher number of ions that grow up the electrical carriers population and to dissolve the oxide layer that reach a dynamic equilibrium on the oxidized surface.

Two electrodes are electrically connected and partially immersed in the electrolyte. In this work a potential is applied between a cathode (Pt foil) and an anode (Sn foil). The applied bias is positive, therefore the cathode (Pt) is the negative electrode. Platinum has a high chemical resistance, so the solution does not damage it during the periods when the potential is not applied. Furthermore, it has a very low electrical resistance, and that enhances the electrical conduction. It performs hydrogen evolution if the applied potential is sufficiently high; this chemical reaction influences the initial step according to the solution pH [32]. According to the established bias definition, the anode is the positive electrode; and it is a tin foil. The oxygen atoms oxidize the tin and generate a combination of stannous  $SnO$  and stannic oxide  $SnO_2$  on its surface. Tin anodization usually is performed using Oxalic acid  $H_2C_2O_4$  or Sodium hydroxide  $NaOH$ , the second is chosen in this thesis. Three different reactions happen simultaneously on the anode[31].



The first reaction equation (2.1) is the formation of  $SnO$ ; the second equation (2.2) is the oxygen evolution that would occur during the reaction because the standard electrode potential is much higher than stannous oxide reaction potential. The oxygen evolution has a predominant role in the nanotube / nanopores morphology creation. The third reaction equation (2.3) dissolves the stannous oxide and creates a dynamic equilibrium that regulates the oxide thickness. The equilibrium favors the oxidation or the dissolution according to the applied potential.

The applied bias rules also the reaction described in equation (2.1), through the Nernst's equation 2.5 that modifies the reaction's Gibbs free energy. The Gibbs' free energy equation 2.4 relates the cell potential resulting from

the reaction to the equilibrium constant. This equation is valid for a reversible reaction.

$$\Delta G = -zFE \quad (2.4)$$

The electrochemical potential ( $E$ ) related to a redox reaction is associated to the Gibbs' free energy variation ( $\Delta G$ ) per charge transfer, where ( $F$ ) is the Faraday constant and ( $z$ ) is the number of exchanged electrons.

The Nernst's equation relates the reduction potential of an electrochemical reaction to the standard electrode potential, which is the measure of an individual potential of reversible electrode at the standard state. It is depending by temperature, electrolyte concentration and chemical species activities. This equation assumes that the electrolyte has a low concentration.

$$E = E^0 + \frac{0.059V}{z} \log_{10} \left( \frac{a_{Ox}}{a_{Red}} \right) \quad (2.5)$$

Where  $E$  is the potential at those conditions,  $E^0$  is the standard potential and  $a_{Ox}$  and  $a_{Red}$  are respectively the concentration of oxidizing molecules and reducing ones and  $z$  is the number of transferred electrons.

According to the relative critical potential position of the two reactions (Eq. 2.1 and Eq. 2.3), one of them is favoured, as shown in Figure 2.2.

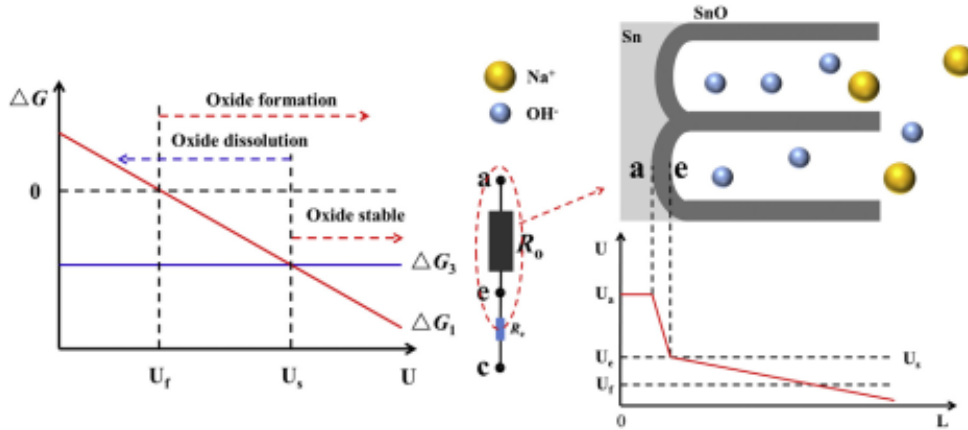


Figure 2.2: Thermodynamic analysis of formation and dissolution of tin oxide and nanoporous structures formation [31].

$U_e$  is the potential at the tin oxide and electrolyte interface. The oxide starts

to grow if  $U_a$ , that is the applied potential, is higher than a value  $U_f$ , which is the voltage required to move the reaction Gibbs' free energy at least to zero ( $\Delta G = 0$ ) (2.1).  $U_s$  is the voltage that ensures the stable formation of pores because it is high enough to unale the dissolution reaction. Both the reactions (Eq.2.1 and Eq.2.3) operate when the potential is between  $U_f$  and  $U_s$ .

The oxide grows at the beginning, but it modifies the electrical behaviour because it adds an increasing resistance that will result in a potential drop, which is proportional to the oxide thickness. If the barrier layer rises the applied potential decrease proportionally. If it is smaller than dissolution potential, the oxide stop to grow and the dissolution reaction began dominant decreasing the oxide thickness and therefore its equivalent electrical resistance. It generates an equilibrium the thickness does not further grow, and the oxide surface potential is dominated by  $U_e = U_s$ .

The growth of the oxide can be monitored by recording the current-time profile, as the applied potential generates a characteristic current profile, shown in Figure 2.3.

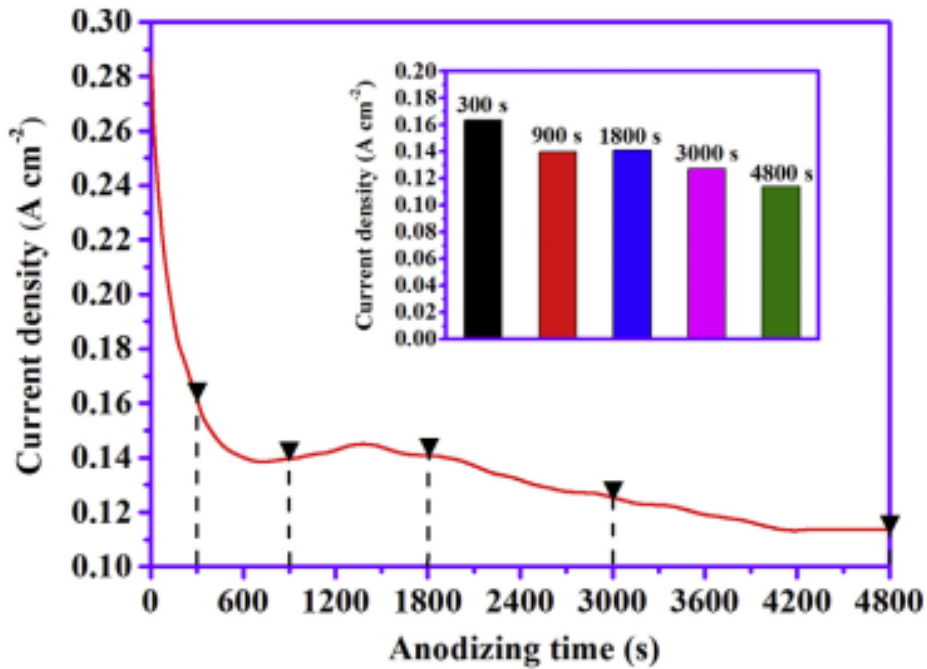


Figure 2.3: Current density vs. time curve at 0.3M at 12V, 25°C [31]

The trend is characteristic for all experiments, but time intervals and current density values depend on many parameters. At the beginning, the current

density is high thanks to the tin conductivity, the electric field at its interface grows up. It attracts the hydroxide anion, that reacts with the metals and generate tin oxide nucleus [31].

According to Figure 2.3 tin starts to oxidize, it generates a compact passivated layer or also called barrier layer, that decreases the electrical properties of the anode and the current transfer drops drastically.

When the barrier layer reach its maximum thickness, then the pores start to grow. They are created by the high electronic current, which generates oxygen nanobubbles at the electrolyte/oxide layer, but also inside the oxide or at the metal/oxide interface [33]. The nanobubbles generated inside the oxide layer can diffuse through this layer, which might increase the plasticity of the layer. It is created by the high ionic current inside the oxide layer, therefore the growing oxide can behave like a viscous fluid. The electrostatic stress in the oxide might allow to overcome the surface tension, so, the nanobubbles generated inside the oxide layer can expand their size accumulating gaseous  $O_2$  [33]. The bubbles obstacle the ionic migration, therefore the anodic oxide will grow only around them. The continuous oxygen release might be responsible of the pores formation. The alkaline electrolyte etches the outer oxide layer [33]. The pores wall are composed by tin oxide crystals with a random orientation, they have are crystallographically interconnected in a chain-like structure [28].

After 300s the structure reaches the equilibrium condition, and the pores increase their size and depth [31]. The tin oxide layer has got quite good electrical properties thanks to the oxygen vacancy given by the non-stoichiometric of the oxide it works like n-type doping. The oxygen leakage allows an increase of unbounded electron concentration that rises the allow electrical carriers, so it reduces the electrical resistivity.

According to Figure 2.3 the oxidation speed starts to decrease after more than 1200s because the hydroxide anions concentration decrease at the metal tin interface. More deep are the pores, and more limited is the mass solution transfer and then smaller is the oxidation speed. It drastically reduces the current density [31].

The anodic oxidation is applied to many other metals, and the resulting material is often in the form of straight nanotube. This is true for titanium and aluminium. The anodic oxidation of tin does not result in straight nanotube, and therefore these are named pores. Many parameters rule the pores size and depth, they are described in the next paragraphs.

- **Applied potential**

Various potentials have been applied for the preparation of the tin oxide via anodic oxidation.

- For potentials above  $5V$  the current density versus time curve always has the same trend. This value corresponds to the material transpassive region; it is the smallest potential to whom start a rapid oxidation [34].
- Under that potential, the anodization speed is low; it generates close pores by the low oxygen evolution; the oxidation reaction is not mass transfer limited. The nanotube-like structure is possible under  $5V$  it has got a straight wall and few structural defects [35].
- Above  $5V$ , the pore creation is dominated by the oxygen evolution; it damages the wall of the pores and creates horizontally cracks. These slots allow a better solution diffusion in the nanostructure, but obviously, they reduce the mechanical strength of the oxid. Potential higher than  $12V$  or for lower potential but with a very long process time the final pores are shallow because upper layers go away [31].

In more detail, for potentials over  $5V$ , a linear trend is observed for average current density and diameter as a function of the applied potential. This is shown in Figure 2.4, where these trends are shown for an experiment performed at  $25^{\circ}C$ , in the  $0.3M NaOH$  at varying applied potential. Samples anodized at applied potential between  $8V$  and  $20V$  have a linear trend. It suggests that the reaction suffers the electrolyte mass transfer limitation, according to Figure 2.4a [31].

The higher is the applied potential to the anode; more charge would participate in the pore initiation and oxygen evolution, then the diameter enlarges, the results are reported in Figure 2.4b [31].

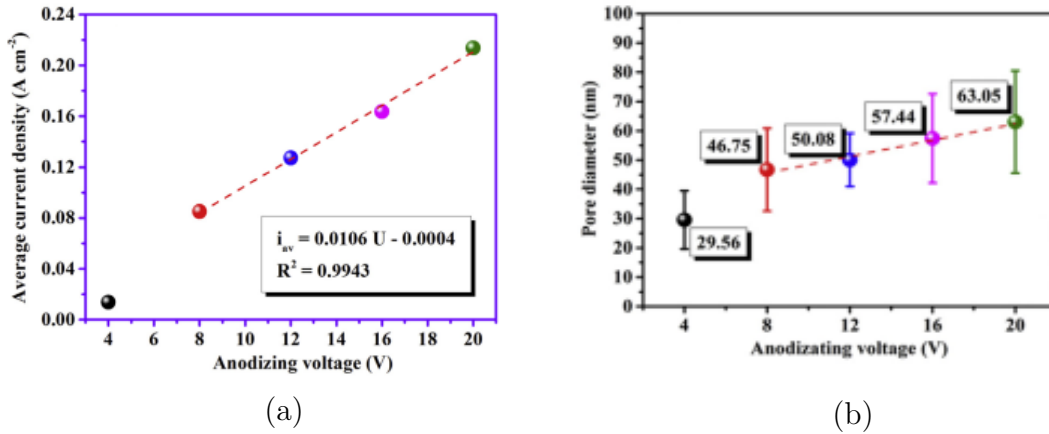


Figure 2.4: Samples analysis at  $0.3M\ NaOH$ , at  $25^{\circ}C$  for different potential (a) Voltage average current relation [31] (b) Pore diameter comparison [31]

The oxide growth rate has got an exponential trend at low applied potential, it remarks the transpassive region up to  $5V$  [34]. Over that value the growth rate is linear as described before. These trends are reported in Figures 2.5.

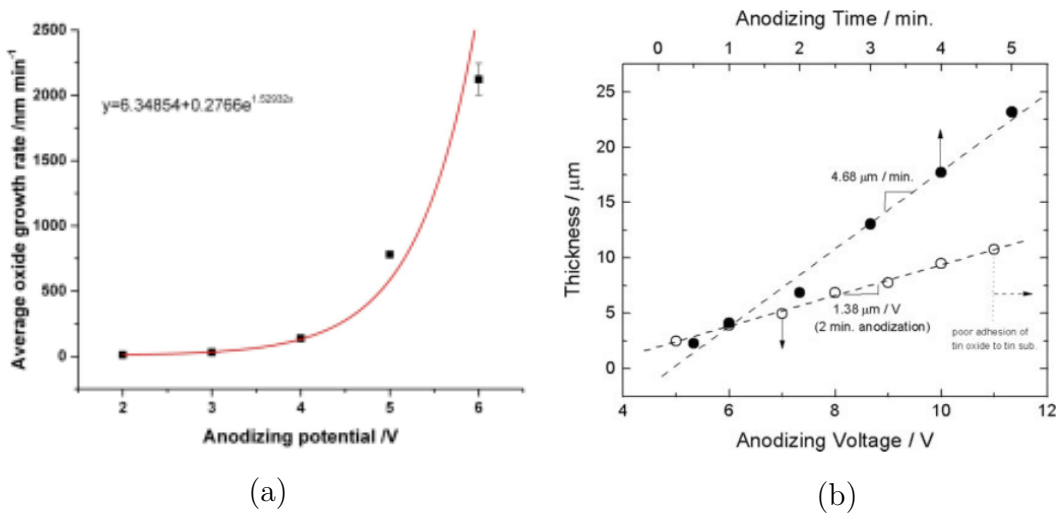


Figure 2.5: Tin anodization growth rate at different conditions: (a) growth rate at low potential [35], (b) growth rate at higher potential: vs time [full dot] and vs applied potential [empty dot] [34].

- **Electrodes distance**

The electrodes distance variation is comparable to a resistance modification; increasing electrode distance, it increases the solution resistance on the equivalent electrical circuit and it decreases the average density current. The electrodes distance is set at 1 cm.

- **NaOH concentration**

The electrolyte concentration has an essential role in the process, and the study of its effect is reported in Figures 2.6 [31].

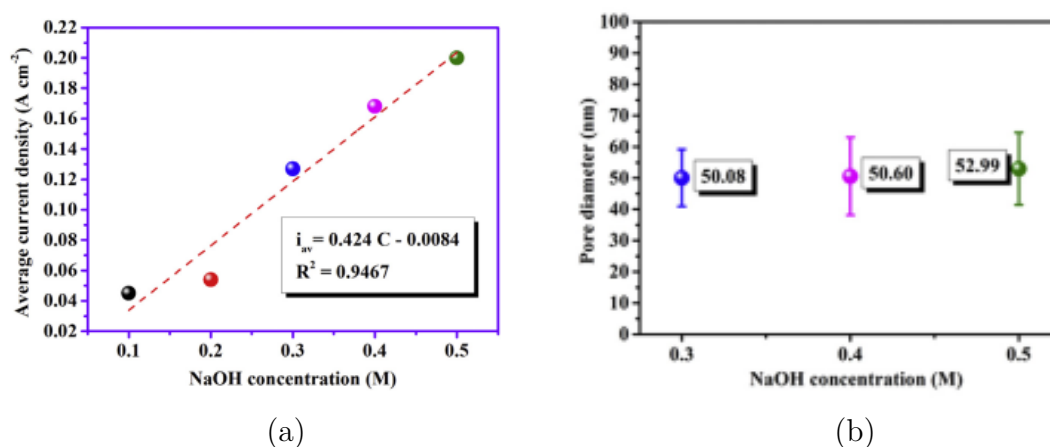


Figure 2.6: Tin anodized reaction at 12V, 25°C at different concentration: (a) average current density [31] and (b) pores diameter [31]

In this reference study the concentration ranges from 0.1M up to 0.5M at a fixed distance for 50 minutes. The average density current has a linear trend; it means that the reaction is mass transfer limited according to Figure 2.6a [31]. With increasing concentration of the solution the diameter of the pores increases, as described in Figure 2.6b. This happens by the enhancement of the chemical etching. The pores size is quite uniform below 0.3M because the concentration of the electrolyte is low; the excess electrolyte concentration would result in the acceleration of diffusion rate and reaction velocity [31].

- **Temperature**

The temperature has a crucial role in the anodic oxidation. The higher is the temperature, and faster the equilibrium condition will be established. Figures 2.7 shows the values of average current density and average pore diameter of the films oxidized at different temperature, keeping constant

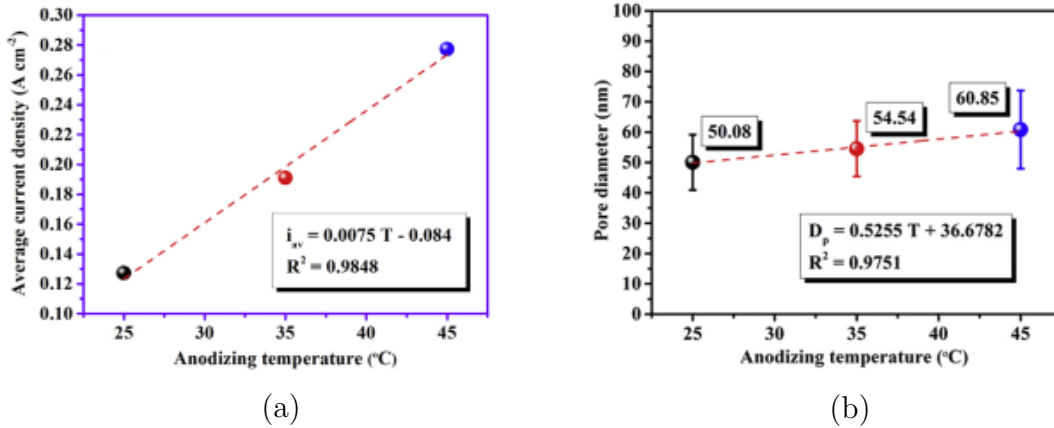


Figure 2.7: Temperature effects, during the anodic oxidation of tin, on: (a) average current density and [31] and (b) average pore diameter [31].

other process parameters ( $0.3M NaOH$ ,  $12V$ ,  $50min$ ).

The pore diameter increases as temperature grows but also the average density current. They are ruled by a linear trend that stress the mass transfer limitation of the reaction. A temperature increase enhance the molecules solution speed, and it favours the diffusion of the molecules reducing the mass transfer limit [31].

- **Stirring**

Stirring the solution enhances the solution exchange inside the pores. This results in a higher current density and more uniform oxygen removal and heat dissipation.

Figures 2.8 shows the influence of the stirring on the average density current and the growth rate at different electrolyte concentration at  $4V$ , and at  $5V$ . This means under and over the transpassive region.

The stirring effect is evident only in the second case because at these last applied potential the oxygen evolution plays a key role. Using this method the average current density and the growth rate at low Sodium hydroxide concentration are increased. At high electrolyte concentration above  $1M$  the growth rate with stirring is reduced because it enhances the dissolution reaction more than the creation [33].

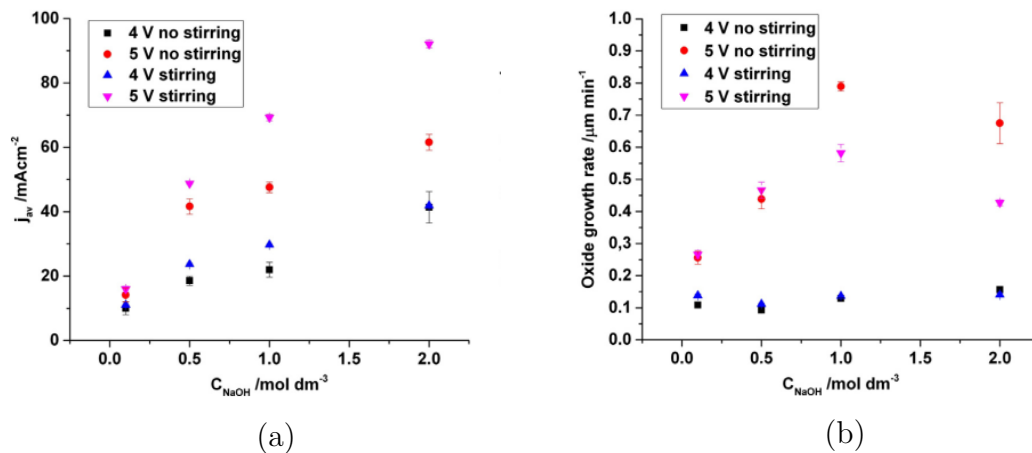


Figure 2.8: Influence of the stirring on (a) average current density [33] (b) growth rate at different potential and as a function of electrolyte concentration [33]

## 2.2 Doping

Structure and morphology of tin oxide-based materials can play a decisive role in enhancing the catalytic properties. A great number of methods have been developed to prepare nanostructured tin dioxide ( $\text{SnO}_2$ ) catalysts for  $\text{CO}_2\text{RR}$ , and it was prepared with various structures:  $\text{Sn}/\text{SnO}_2$  porous hollow fiber [18],  $\text{SnO}_2$  nanosheet/Carbon cloth [19], tin oxide with different oxidation state ( $\text{SnO}_x$ ) nanoparticles [20] and Sn dendrite [25].

It is however desirable to further improve catalytic behavior of this material. According to the theoretical work of Karthikeyan Saravanan and coworkers [29], the introduction of substitution dopants close to the surface, and therefore their positions near to adsorbing sites (depending on the elements either a six-coordinate Sn atom at the surface or Sn atom next to an oxygen vacancy defect) can result in a decreasing of the  $\text{CO}_2$  reduction over-potential. It might be possible through a different binding energies of reaction intermediates, which in turn affect the overpotential. The elements, which are predicted to show the best improvement, include titanium, vanadium cadmium, zirconium, niobium and zinc [29]. It was also shown that the catalytic properties of the tin based catalyst can be improved by homogeneous doping of Ti into the lattice of  $\text{SnO}_2$ , which prevents the recombination of electron-hole pairs and expands the range of usable excitation light to the visible-light region [36].

The doping is used to introduce a certain number of atoms, in a crystal structure. They might alter the electrical properties, changing the carrier population, if doping atoms have a number of electrons in the outer shell different from the bulk material. If there are electrons in excess, the electrons population increase, otherwise the holes population rise up.

Doping atoms need to be activated, they have to become substitution impurity, chemically bound to the other atoms inside the crystal lattice. If the impurities have a significantly different size comparing to bulk atoms, they introduce also stress in the lattice. In certain cases it might increase the conductivity thank to the energy bands curvature distortion.

The technologies chosen for the introduction of the doping in this study are the Atomic Layer Deposition and the Impregnation technique.

- **Atomic Layer Deposition (ALD)**

ALD is the technological evolution of chemical vapour deposition. The chemical reaction is divided into two half-reactions, and the precursors are separated. The set up consists in a chamber at low pressure, a gas flow control system and a heating plate that hosts the target sample. When the gaseous precursor is injected inside the chamber it diffuses and then it is chemisorbed by the sample surface. When all the possible binding sites are filled no other atoms can bind to the surface. It is, therefore, a self-limiting reaction [37].

In the case of oxides deposition, the first injected precursor at high temperature and low pressure is water vapour that flows to the target surface. The substrate is heated to provide the activation energy required to create a chemical bond. At the end of this process the surface exposes hydroxide groups. Subsequently the gas is purged through an inert gas flow, it removes the previous precursor and after, injecting the next desired one, the process is repeated.

Precursor could be a metal atom bound to some methyl groups or to an halogen atom. It reacts with the hydroxide groups on the surface and with their hydrogen atom and a methane or acid molecule is released [38].

This technology guarantees a mono-layer precision, so it is possible deposit the desired thickness repeating the process a certain number of times. The precursors need to be volatile, thermally stable and have a quick reaction with the previous layer. Usually, precursors are very reactive molecules [37].

Each material has a characteristic growth rate at a particular temperature. ALD have many advantages, a big control on the deposited thickness and an optimal uniform deposition both inside nanotube and porous structure, with an aspect-ratio higher than 2000:1 [39].

- **Impregnation**

This method is based on putting in contact metal with a solution rich of desired doping atoms. At the interface between bulk and solution, different reactions take place, including selective adsorption of species by van der Waals or H-bonds, ion exchange if the surface is charged, and also the partial dissolution of the surface. The reaction depends on the solvent, on the substrate, and other parameters, among which pH is the most important. These parameters control the ionization and the solvation.

The surface topography can influence the deposition property. Good dispersion is difficult inside high aspect ratio structures, and it depends on their aperture diameter. This could be an issue for the material studied in this thesis, which is porous. However, the pores are quite large, and the solution can also enter through numerous cracks. In any case, this method ensures good control of the deposited species and a high dispersion over the surface.

The doping atoms deposition depends on the solid/liquid ratio, and it is strictly related to the equilibrium condition. When the precursor, that contains the doping atom, is introduced in a water solution, it undergoes a hydrolysis reaction. The pH has an important effect on the metal oxide molecules creation. These last diffuse in the solution, that is continuously kept in agitation thanks to stirring, are adsorbed on the surface[40].

These two methods, at this point, can create a new layer on the existing tin oxide surface. To intercalate the doping atoms inside the initial structure a heating treatment is required. The annealing post-process provides the diffusion of the atoms inside the tin nanoparticles creating substitutional impurities.

## 2.3 Annealing

Annealing is a heat treatment that favours atoms reorganization. The high temperature increases the atom vibrational energy. Often it is sufficient to break inter-atomic bonds and modify the atoms disposition and their oxidation state. This process is used to reduce dislocation impurities, and also allows modifying the crystalline structure. Annealing also has another task, it can be used to favour the diffusion of superficial atoms inside the bulk [41]. The temperature increase allows a surface reorganization, atoms can migrate and adsorbed one could generate chemical bonds with substrate atoms and they become impurity defects inside the lattice [41].

Tin is a low melting point metal, 232°C. It is a huge limitation for annealing treatment. Its oxides have a higher melting point, for stannous oxide  $SnO$  it is 1080°C and for stannic oxide  $SnO_2$  it is 1360°C. These two oxide species generate interconnected nanoparticles, which create the walls of the pores. They are nonstoichiometric nanoparticles, with an amorphous lattice rich of dislocation impurities. Heating time, temperature, heating ramp and oxidative atmosphere directly act on the crystal periodicity, removing the dislocation and modifying the oxygen concentration.

It is possible to modify the crystal periodicity and obtain tin dioxide in a tetragonal rutile structure [28].

In this work tin oxide nanostructure is annealed using two different methods, and some considerations, described below, have to be taken into account.

The following described experiments consider annealing for three hours and then the material is gradually cooled [42]. If the temperature is below 400°C it is possible to perform the annealing on the native substrate, it is however necessary to use some precautions (because this temperature exceeds the melting temperature of metallic tin).

The sample can be heated once placed on a copper foil. The metal tin, out of its oxide structure, melts. However, thanks to the adhesion force between the two metals, melted tin does not move away, but generate a pool that protects the oxide substrate. Its exposed surface reacts with atmospheric oxygen and creates a new oxide layer that protects the substrate from further melting [43].

For the annealing at higher temperatures, it is necessary to remove the nanostructured tin oxide layer from the substrate. Otherwise, the oxide layer peels off from the substrate and the nanostructure it is damaged.

At 200°C there is a formation of  $SnO_x$  species, the temperature is not

sufficiently high to change the oxidation state of  $Sn^{2+}$  up to  $Sn^{4+}$ . The temperature of  $300^{\circ}C$  does not entirely convert  $SnO_x$  to stannic oxide, but its concentration increases because of the saturation of the oxygen vacancy. There is also a colour variation, the oxide layer becomes white. Above  $400^{\circ}C$ , the annealing converts all the oxide molecules in a stannic oxide [42]. Further increase in temperature improves the crystallinity of the oxide nanoparticles decreasing the defects and also increase the crystal size.

Annealing Temperature [ $^{\circ}C$ ]	Crystal size [nm]
400	4.1 - 4.5
500	8.3 - 9.1
600	9.0 -9.9

Table 2.1:  $SnO_x$  particles size at different annealing temperatures [42]

The increase of annealing temperature influences also energy band-gap. It shifts from  $2.6eV$  for the amorphous tin oxide up to  $(3.15 - 3.3)eV$  for material annealed at  $450^{\circ}C$ , and with annealing at  $600^{\circ}C$ , the stoichiometric stannic oxide with an energy gap of  $3.6eV$  is obtained.

## 2.4 Field Emission Scanning Electron Microscopy (FESEM)

The samples growth, their morphological characterisation and compositional analysis were performed using a Field Emission Scanning Electron Microscopy (FESEM, ZEISS Supra 40 and ZEISS Auriga), equipped with an Energy Dispersive X-ray spectrometer (EDX, Oxford INCA).

FESEM uses an electrons source to observe the objects, and with this source it achieves the resolution which is under the white light optical resolution. In FESEM an incident electron beam is scanned across the sample's surface and the resulting electrons emitted from the sample are collected and form an image. The advantage of the use of the electrons is that the energy is tunable and much more energetic than white light. All this result in the possibility to observe objects at the nanometric scale.

There are different electron beam sources, which result in a different lifetime and beam intensity. The two electrons extraction methods are: thermionic electron emission or field emission.

In the first case, a filament is heated at a temperature that guarantees to the

outer shell's electron enough energy to overcome the work function barrier. The filament usually is made of tungsten. It has a small work function  $4.5\text{eV}$  that correspond to  $2650^\circ\text{C}$ , that is below its melting temperature. It can also be made of  $\text{La}_6\text{B}$ , which needs a lower temperature of  $1600^\circ\text{C}$  [44].

The second technology is based on a single wire fashioned into a sharp tip. This last is subjected to a very high electric field. It decreases the potential barrier and electrons can escape thank to the tunnelling effects. The filament is made of tungsten. This technology has a generated current ten times higher and the surface is better resolved.

The advantage of field-emission cathode in the electron gun is a narrower probing beam, resulting in improved spatial resolution and minimized sample charging and damage [44]. The generated and accelerated electrons pass through an aperture system used to remove the electrons that are emitted with a spread angle. Subsequently, they are accelerated at the desired energy. They move along a tube where a magnetic lens system rules the focus and the beam diameter, thanks to the Lorentz's law. A raster scan, using a coil system, moves the beam on an X-Y axis.

The interaction of the beam with the sample has a different behaviour depending on the accelerating voltage and the bulk's atoms atomic number. The beam energy determines the penetration depth and the electrons diffusion in the sample volume. If the bulk is composed of light atoms, the beam generates a pear-like diffusion volume with deep penetration. In the opposite case, the electrons interact with the upper surface layer and generate a shallow hemispherical interaction volume [45]. These conditions are shown in Figure 2.9.

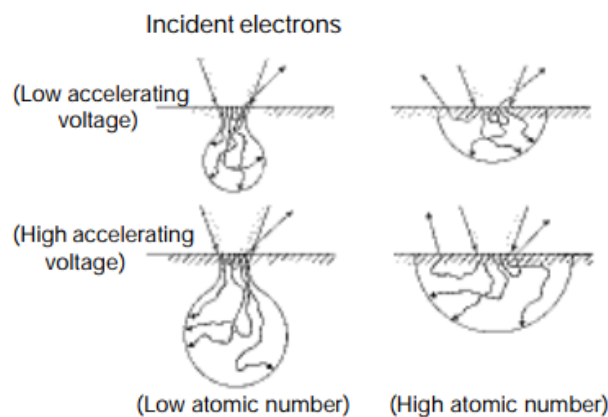


Figure 2.9: Interaction of electrons with specimen, and resulting interaction volume [45].

The incident beam interacts with atom's electrons and generate different effects, the most important are: Backscattering electrons, secondary emitted electrons, X-ray. All of them have different energies and different emission angle. The overview of these processes are shown in Figure 2.10.

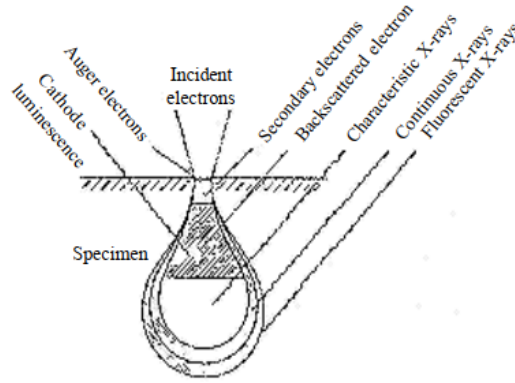


Figure 2.10: The interaction of the beam with the sample [45].

The primary electrons interact with atoms, and this interaction could generate secondary electrons. The diffusion length between the emission position and surface need to be smaller than the mean free path, thus tens nanometers. The secondary electrons are emitted with small energy, they have a high spatial resolution and have a widespread angle. According to their characteristic they carry topographic information [45]. The back-scattered electrons or Rutherford's scattered electrons are more energetic, and they can be collected from deeper interacted atoms. They are generated by the interaction between primary electrons and the nuclei that deflect them back. They are emitted with an angle close to the incoming beam. They are representative of the composition variation within the sample [45]. The X-rays are generated as a result of inelastic interaction of the electron beam with the specimen atoms, and two different types of interaction are possible. Characteristic X-rays result when the electrons beam eject inner shell electrons of the specimen atoms and electrons transition in atomic core levels occurs. And the second, which is continuum (Bremsstrahlung) X-rays result when the beam interacts with the nucleus of the specimen atoms [45].

The different emitted beams are detected with different detectors. Imaging is typically obtained using secondary electrons, which gives the best resolution of the fine structure and surface topographical features, or back-scattered electrons, which give contrast based on the atomic number to resolve sufficiently large composition variations.

FESEM has some limitations for a non-conductive substrate, if the current is too high it cannot dissipate incoming electrons and generates the charge up effect. In this case, there is a charge accumulation on the surface that deflects the primary electrons beam. The field emission electrons source drastically decrease charge up effect. If the primary beam is too intense, it might damage the soft sample [44].

### 2.4.1 Energy-dispersive X-Ray (EDX)

The characteristic X-rays can be used to qualitatively and quantitatively analyze the chemical composition and element distribution in the sample. The X-rays carries chemical composition information. They can be measured using different configurations, but all of them are based on the energy discrimination of the emitted X-rays. A pin junction converts them in electron and hole pairs. The signal depends on the generated current that is proportional to the X-ray intensity. The X-ray energy is like the atom's fingerprint, knowing that value is possible to reconstruct the sample chemical composition.

## 2.5 X-Ray Diffraction (XRD)

X-ray diffraction is a technique that provides information on the sample crystal structure. The X-rays are very energetic, their wavelength is comparable with bulk's atoms interplanar distance. It allows the identification of crystal structure class and its orientation. Analyzing the data is possible get information on grain size.

The X-ray irradiates the sample surface with a specific angle. Atoms' material absorbs the impinging photons according to Lambert Beer's law. The radiation exponentially decreases, increasing the penetration depth. The absorption is proportional to the electron per unit of volume, therefore it depends on their atoms atomic number and packaging factor. In the end, less energetic photons are strongly absorbed [46]. The atoms that interact with X-rays become excited and then they will relax generating another photon with smaller energy, it is almost univocal. According to kinematic approximation [46], any other sample's atoms will not absorb the emitted photons. The emitting atoms are considered as the points-like source of a spherical wave. It propagates and, at the detector plane, can be considered as a plane wave, thank the quite infinite distance. The emitted electromagnetic waves interact and generate constructive and destructive interferences.

The interferogram carries information on the crystal structure. With the position of the detected peak and thanks to database information is possible to determine the crystal structure. Different crystal orientation will have a different peaks position. A monocrystal has a single peak, polycrystalline have different orientation, so many peaks. The dimension and the abundance of the grains determine the peak height and its Full-Width Half Maximum (FWHM). Bigger is the dimension of the average grains and lower FWHM of the peaks.

The crystalline structure can be studied in the real space or in the reciprocal lattice space. The approach is different, but the final result is the same. In the first case, the constructive interference is determined by Bragg's law described by the equation 2.6 [47]

$$2 \cdot d \cdot \sin(\Theta) = n \cdot \lambda \quad (2.6)$$

It studies the diffracted light by atoms set on different planes, where  $d$  is the distance between crystal planes,  $\lambda$  wavelength of X-ray,  $\theta$  incident angle and  $n$  is the diffraction order. There is constructive interference only at some angles with a certain periodicity.

The Laue's law is Bragg's law respective in the reciprocal domain it is described by the equation 2.7 [47].

$$\vec{k}' - \vec{k} = \vec{G} \quad (2.7)$$

$\vec{k}$  they are the wavevectors of the incident and scattered X-rays, they are assumed monochromatic and  $\vec{G}$  is the reciprocal lattice vector. It means that wavevectors need to be the same, in modulus. Their difference is equal to the reciprocal lattice vector.

Several possible diffraction geometries can be used to obtain various information about the crystal, the most commonly used is the Bragg-Brentano, there is also the "Thin-film" configuration. In the first case, X-ray source is fixed, instead sample and detector change their angle. A widespread angle range is scanned and the intensity related to the constructive interaction is converted in an electrical signal proportionally to the intensity.

The Thin-film case keeps fixed the impinging angle. It modifies the detector angle to collect all the generated X-ray.

XRD was performed to determine the crystalline structure of the catalysts. It was used in BraggBrentano symmetric geometry by using a PANalytical X'Pert Pro instrument (Cu K radiation, 40 kV and 30 mA) equipped with an X'Celerator detector.

# Chapter 3

## Introduction to electrocatalysis

### 3.1 Electrochemical reduction of carbon dioxide $CO_2RR$

Carbon dioxide is a very stable molecule, it has a double covalent bond between the carbon atom and each oxygen atom. The molecule has a planar configuration with an angle between the two oxygen atoms equal to  $180^\circ$ . The chemical bonds and the structure guarantee high stability with Gibb's free energy of  $\Delta G = -400Kj/mol$ . The molecule structure has a high symmetry that avoids the net charge localization, thus it is an apolar molecule. It is possible thanks to the opposite interaction given by the two oxygen atoms, where one compensates the other [48]. It is usually the product of the oxidation of organic compounds and hydrocarbons.

The conversion of these waste molecules in a reusable chemical reagent attracts huge attention within the scientific community. Its reduction into valuable fuels is possible using different approaches such as: high pressure and temperature reaction, photocatalytic reaction and electrochemical reaction. The last two are based on electron transfer and carbon dioxide reduction. The semi-conducting electrodes instability limits the photon-based reactions [49]. The electrochemical process is widely studied and it is predicted to be applied in industrial application [11].

The electrochemical reaction uses a stable catalyst that transfers electrons from an inexpensive, abundant molecule like water to the carbon dioxide. The process can be divided into two half-reactions: the cathodic one is the

carbon dioxide reduction and the anodic one is the water oxidation, some reaction products are reported in the Table 3.1.

Oxidation process	Reduction process	$\Delta G_{rxn}^0$ [kJ/mol]
$2H_2O \rightarrow 4H^+ + 4e^- + O_2 \uparrow$	$4H^+ + 4e^- \rightarrow 2H_2 \uparrow$	474.33
$H_2O \rightarrow 2H^+ + 2e^- + 1/2O_2 \uparrow$	$CO_2 + 2H^+ + 4e^- \rightarrow CO \uparrow + H_2O$	257.38
$H_2O \rightarrow 2H^+ + 2e^- + 1/2O_2 \uparrow$	$CO_2 + 2H^+ + 2e^- \rightarrow HCOOH$	269.86
$3H_2O \rightarrow 6H^+ + 6e^- + 3/2O_2 \uparrow$	$CO_2 + 6H^+ + 6e^- \rightarrow CH_3OH + H_2O$	701.87
$4H_2O \rightarrow 8H^+ + 8e^- + 2O_2 \uparrow$	$CO_2 + 8H^+ + 8e^- \rightarrow CH_4 + 2H_2O$	818.18

Table 3.1: Some products of  $CO_2RR$  half-cell reactions and their standard Gibbs energy of formation [49].

The water-splitting reaction provides electrons and hydrogen cations, both are attracted to the cathode. The anode absorbs the first and they flow in the electrical circuit. Instead, protons diffuse through the electrolyte. The reduction reaction consumes electrons and hydrogen cations. It generates a diffusion gradient, but the total concentration is always constant. At the cathode, two competitive reactions exist. They are carbon dioxide reduction and hydrogen evolution, one dominates on the other according to the reaction condition and applied potential.

Half-cell reactions contribute to the theoretical standard cell potential. It is the sum of the reaction potential required at the cathode and anode according to the equation 3.1.

$$E_{cell}^0 = E_{cathode} - E_{anode} \quad (3.1)$$

The half-cell potential is related to the Gibbs' free energy according to the equation 2.4. The Gibbs' free energy depends by the reaction condition and compounds involved according to the equation 3.2.

$$\Delta G = \Delta H - T\Delta S \quad (3.2)$$

The Gibbs' free energy depends on the enthalpy ( $H$ ) and the entropy ( $S$ ) of the reactants and products reaction, and its temperature ( $T$ ). The relation between the standard potential and the Gibbs' free energy depends on the number of exchanged electrons [49]. The final products are strictly related to the catalyst under analysis, the number of electrons involved in the reaction and the applied potential [17]. These last depend on the overpotentials required to obtain the reaction intermediates [17].

The pH directly influences the reaction potential according to the equation 3.3 [49].

$$V_{RHE} = V_{ref} + 0.059 \times pH + V \quad (3.3)$$

Where  $V_{RHE}$  is the standard reference potential,  $V_{ref}$  is the used reference electrode and  $V$  is the applied potential [50]. Equation 3.3 allow to convert the applied potential measured with different reference electrodes to a standard value, the Reversible Hydrogen Electrode, (RHE).

The pH distribution is not uniform in the whole cell. Its gradient is related to the protons flow, generated by the reactions at the electrodes, described in the table 3.1.

Carbon dioxide introduced in the solution might react with water. The  $CO_2$  has a slightly positive charge accumulated on the carbon atom created by the electronegative difference between oxygen and carbon atoms. It creates an electrical interaction with the net negative charge on the water's oxygen atom. It is a van der Waals interaction that generates a nucleophilic reaction. The electrical interaction begins a chemical bond shearing electrons. Water loses a hydrogen atom that reacts with carbon dioxide's unstable oxygen. This process generates a carbonic acid molecule. The reaction steps are described in the following Figure 3.1.

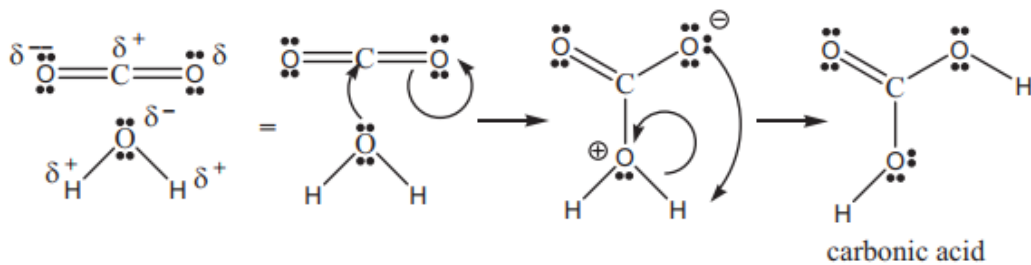


Figure 3.1: Formation of carbonic acid from dissolved  $CO_2$  molecule in an aqueous solution [49].

The reaction has a slow kinetic, thus it has a small equilibrium constant. Only 0.2% – 1% dissolved carbon dioxide molecules are converted at the equilibrium. The carbonic acid might lose the hydrogen atoms and therefore increase the solution acidity. This reaction is not kinetically favoured. It can be considered negligible at room conditions compared to the amount of solvated  $CO_2$ , but the carbonic acid dissociation might generate a significant pH variation [17]. A further dissociation of the carbonic acid is limited by

the very small dissociation constant [49].

Henry's law, equation 3.4, determines the gas solubility, it is strictly dependent on the reaction condition.

$$\rho_{CO_2} = K \times X_{CO_2} \quad (3.4)$$

Where  $\rho_{CO_2}$  is the partial pressure of the gas in the atmosphere,  $K$  is a constant of the gas and  $X_{CO_2}$  is the equilibrium mole fraction of gas ( $CO_2$ ) in liquid phase [49]. In a neutral solution, the carbon dioxide concentration would be  $34mM$ . However, for various electrolytes, and any changes in pH this value will be different and can be as low as  $3.5\mu M$  [17]. Electrolytes like  $KHCO_3$  or  $K_2HPO_4$  and others have a buffer effect that reduces the pH variation at the electrode interface during the electrochemical reaction [49]. The pH variation is strictly related to the carbon dioxide concentration. The electrolyte's cations radius has an important role in the chemical reaction path [17].

The  $CO_2RR$  is strictly related to the catalyst used and reaction condition. Many metals and their oxides perform hydrogen evolution; some others like zinc, silver, gold generate carbon monoxide. And tin, indium and lead's main product is formic acid. Copper has got a multivalent action: it might produce multi-carbon hydrocarbon, carbon monoxide but also alcohols according to the reaction conditions [17]. In this work, the focus is  $SnO_2$  based electrode. Tin has got a better electrocatalytic performance if it is oxidized, and it was demonstrated that its catalytic efficiency might be increased by 15% up to 60% at a  $-0.7V vs RHE$  [17]. Tin oxide and indium oxide, are classified as active oxides [17].

During the reduction reaction tin oxide does not reduce completely and an oxide interface always remains present [51]. This is called meta-stable oxide, and the oxide layer is reversible and during the operation condition, it continuously changes its thickness and oxidation state [51].

There is a number of events occurring on the catalyst that must happen in consecutive way in order to perform successful reduction and conversion process. This includes  $CO_2$  adsorption, intermediates formation, and product removal from active sites. The carbon dioxide adsorption on the surface is a crucial step for the reduction reaction path [16]. It drastically decreases the reaction activation energy of the carbon dioxide reduction comparing to start from the isolated molecule. There is a number of products created during the conversion process with the use of tin oxide. Tin oxide might produce hydrogen, formic acid or carbon monoxide. Which one is produced depends

on the reaction conditions, especially by the applied potential; at small negative one the Hydrogen Evolution Reaction (HER) is favoured. The reaction to obtain these two products involves two protons and two electrons transfer. Different possible reaction paths are described in Figure 3.2 [16].

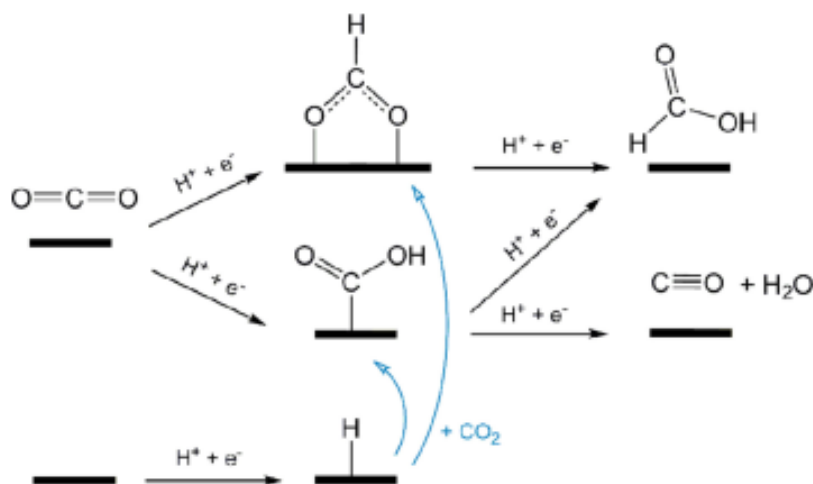


Figure 3.2: Possible reaction path for  $CO_2$  reduction to formic acid [16].

Tin oxide surface might interact with the  $CO_2$  molecule in different ways, the most active sites are the surface defects and the oxygen vacancy. These last are the more stable, according to the thermodynamic data. The reaction intermediates for carbon dioxide reduction requires one electron transfer and the absorption of a proton, to stabilize them. It is possible with an applied bias, thermodynamically it needs only  $-0.17vsRHE$  [16], but in the real case higher potential is required for carbon dioxide.

Depending on the  $CO_2$  bonded atoms to the surface are possible two different reaction intermediates: the carboxylate ( $COOH^*$ ) and the formate ( $OCHO^*$ ) [16]. Also, the carbon dioxide interaction with adsorbed hydrogen atom might produce these reaction intermediates. They have a different chemical reaction path and also different intermediate activation energy. The two possible compounds react with another proton and another electron to generate formic acid. The  $OCOH^*$  intermediate might produce either formic acid or  $CO$ , it is related to the adsorption strength and reaction condition. The carbon monoxide production release also a water molecule. These reaction processes are described in Figure 3.2.

The previous reactions have a Tafel slope of  $120mV/dec$  [16], so it is an

index that the first electron transfer to carbon dioxide anion is the rate-determining step. Recently other studies suggested a different Tafel slope ( $60\text{mV/dec}$ ) [16], it indicates that the rate-determining step is the proton transfer. Another study based on anodized tin focused the attention on grain boundary defects as active reaction sites. The tin oxide obtained by the anodic oxidation is porous, and walls are made of a conglomeration of stannic oxide nanoparticles. Nanoparticles have different lattice orientation, and they are crystallographically interconnected [28]. It was shown that the dimension of nanoparticles plays an important role in the formic acid conversion,  $5\text{nm}$  was shown to be the best dimension, formic acid production decreases increasing particles size [49]. In the materials with grain boundaries, the increasing particles size result in a decrease in particles number and also it decreases the overall grain boundary exposed area.

The faradic efficiency is a parameter used to describe the charge transfer efficiency from one system to another compound. Usually, it is referred to a single electrochemical reaction because different compound might need different parameters or a different number of exchanged electrons. The equation 3.5 [11] describes this value.

$$\epsilon_{Faradic} = \frac{z \cdot n \cdot F}{Q} \quad (3.5)$$

Where  $n$  is the number of final product molecules,  $F$  is the Faraday's constant and  $z$  is the number of required electrons to perform the electrochemical reaction.

## 3.2 Electrochemical set-up

The set-up comprises an electrochemical cell, three electrodes, an ion exchange membrane and a power supply. The electrodes are: working electrode, reference and counter electrode. The working electrode carries out the electrochemical events of interest. In the case under analysis, it is composed of  $SnO_2$  mixed with acetylene black carbon and Nafion deposited on a carbon paper GDL. It adsorbs the reagent on its surface and then through an electron transfer, it modifies the adsorbed species to obtain the final products. The potential is applied between the working and the counter electrode. This last is usually a platinum wire, it is used to close the electrical circuit [52]. The reference electrode has a specific and stable equilibrium potential. It is independent of the variation in the electrochemical cell. It is used to keep the potential at a fixed value even if the external condition might change, or to have information on external condition variation. There are different standard references like Reversible Hydrogen Electrode, Saturated Calomel Electrode or  $AgCl/Ag$ . This last is widespread, and it is used in this thesis. It is composed of a silver wire immersed in a standard electrolyte solution,  $3MNaCl$ . The silver ions conversion, in this case, is printout. Therefore its potential is always at a fixed value. To detect the reaction condition and possible variation, the standard electrode is in contact with the external solution through a glass frit tip [52]. The cell potential might change according to a pH variation. In order to have a standard and reproducible experiments usually, the potential is referred to RHE, if the potential is evaluated with different reference electrodes it can be converted using the Equation 3.6 [50].

$$V_{RHE} = V_{ref} + 0.059 \times pH + V \quad (3.6)$$

Where  $V_{RHE}$  is the standard reference potential,  $V_{ref}$  is the used reference electrode and  $V$  is the applied potential [50]. This three electrodes system generates a specific resistance, which determines the Open Circuit Potential. This last is the highest applied potential which does not generate a current flow. It is determined by electrodes conductivity, their distance and the electrolyte conductivity. During the measurements, the 85% of its resistance is compensated [52].

The most common reactor uses a liquid medium to perform carbon dioxide reduction.

In the initial experiments, a single cell was used, and the electrodes were in the same chamber. This leads the diffusion to the anode and the oxidation of  $CO_2$  reduction products. To avoid this problem, a physical barrier

in the form of the ions exchange membrane was introduced [53]. It divides the working cell into two reaction chambers. This last configuration varies according to how the carbon dioxide is introduced [53]. In Figure 3.3, two cells configuration are reported.

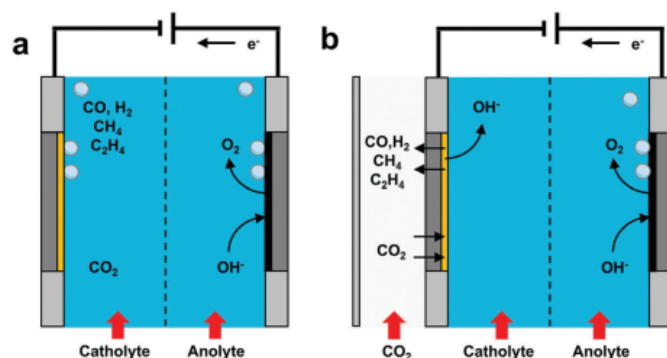


Figure 3.3: Different electrochemical cell configurations [53].

The H-cell Figure 3.3 a has a gas stream bubbled in the electrolyte. Carbon dioxide diffuses in the solution, according to Henry's law (as described before). Then it diffuses towards the cathode surface thanks to the different concentration. This happens because it is a reaction reagent, and it is consumed on the electrode surface. The other configuration shown in Figure 3.3 b uses a gas diffusion layer as electrode support. The carbon dioxide stream is injected into the solution, passing through the electrode substrate. Carbon dioxide is injected behind the electrode surface, and then the reaction products move out from the same side. Instead, the water reaction is always in the liquid medium like Figure 3.4 shows.

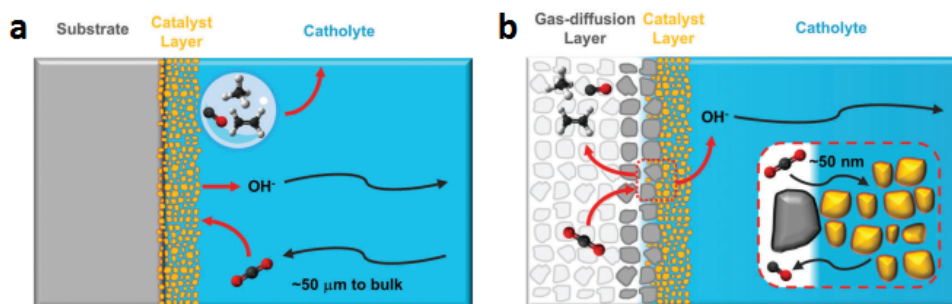


Figure 3.4: Carbon dioxide and reaction products different diffusion path. a) H-cell electrode [53] and b) gas diffusion layer electrode [53].

There is a substantial difference between these cells. The H-cell requires a

higher gas stream to have enough carbon dioxide at the electrode interface. The gas diffusion layer technology might use a gas stream one thousand times smaller, but its production rate can result even higher [53]. This happens because in the second case, the gas diffuses inside the electrode and then it is immediately available at the electrode electrolyte interface.

In both cases, the hydronium ions consumed by the carbon dioxide reduction generate an increase of hydroxide anions. The leakage of protons is a reaction limitation. The pH variation might modify the reaction path and carbon dioxide availability. But more importantly, it induces a change in the source of protons, from hydronium to water-splitting [53].

There is also a significant variation in the maximum predictable current density for the two systems. The maximum current for H-cell is  $35\text{mA}$ , while in gas diffusion technology the current density might rise to  $200\text{mA}$ . It directly acts on the solution pH and obviously on the carbon dioxide concentration in solution. The four Figures a-d 3.5 show the variation of these parameters at different current density values.

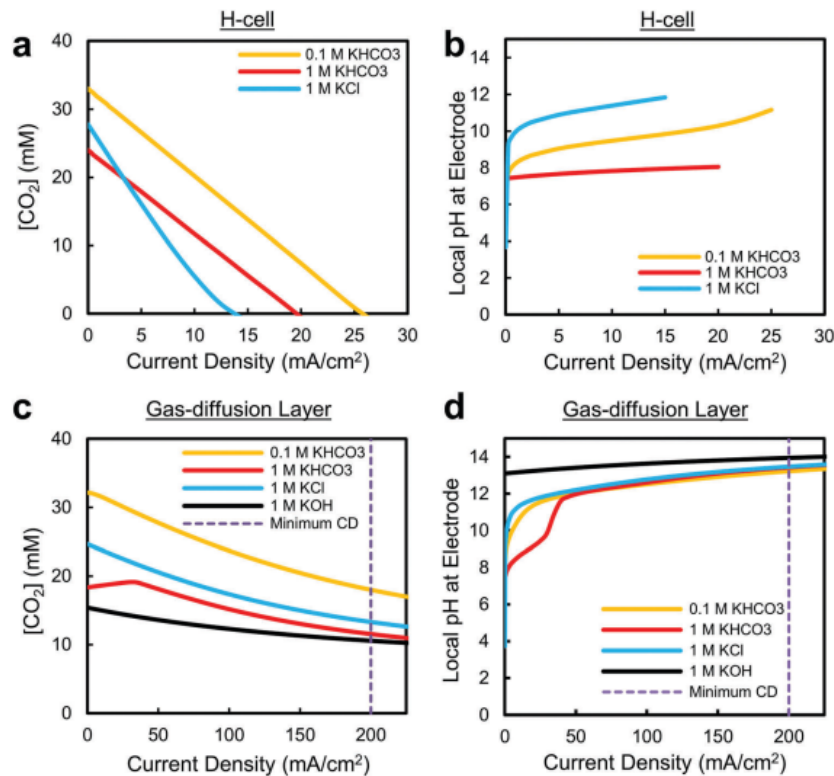


Figure 3.5: a) and c) shows the carbon dioxide concentration in the two technologies [53], b) and d) shows the current value for both [53].

The gas diffusion layer cell has a better carbon dioxide diffusion, even its gas stream is a thousand times smaller. Its current range is almost one order of magnitude higher [53].

This thesis uses an H-cell configuration, the electrolyte behaviour was already described in the previous section. Shortly, its main tasks are to improve the carbon dioxide solubility and buffer the hydroxide ions generated at the anode interface.

The ions exchange membrane might be cationic or anionic. In this case, the focus is set on proton exchange membranes, like the Nafion one. A fixed charge concentration characterizes it. The higher it is, the better are the conductivity properties. They are determined by the active sites, made of  $SO_3$  [54]. They determine the equivalent weight (EW), which is the polymer weight per mole of active sites, and it is inversely proportional to the ions exchange capacity. An optimal EW is between 900 and 1350g/eq [54]. The membrane thickness is inversely proportional to its ability to exchange gas, but it is directly proportional to its conductive properties [54].

Its protons exchange ability is also strictly related to its hydration, which is the measure of the water molecules per active site [54]. It was theorized that in the humidified membrane, aggregates of solvated ionic sites, called cluster, are formed. When clusters interact, they create a percolative path with a nanometric channel of 1 nm in diameter. It interconnects the different clusters and allows the protons exchange [54].

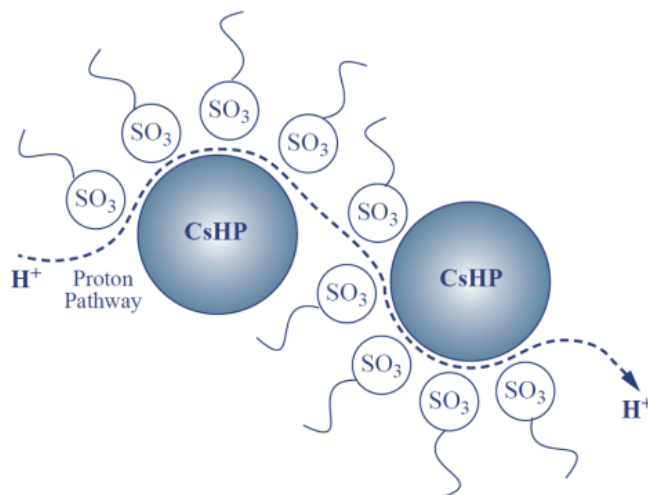


Figure 3.6: Nafion percolative protons path [54].

The last but not least components are the electrodes. The cathode is the

tin oxide electrode, the anode is a conductive metal like platinum and the reference electrode, in this case it is  $Ag/AgCl$  with an electrolyte solution  $3M NaCl$ . The electrodes for  $CO_2RR$  are fabricated in a different way, depending on the cell configuration. This work uses an H-cell, therefore only this last case will be studied in depth in this thesis.

Here there are two examples of the preparation of the electrodes and obtained results with the use of anodic tin oxide.

- In the first case, the tin oxide grows on its substrate using an anodization technique. The obtained surface will be the electrode, it is self-standing. This method has some limitations because when the applied potential overcomes the tin reduction potential during the  $CO_2RR$ , the upper layer of tin oxide peels off. Only a part of the tin oxide structure stays on the substrate. In this electrode best case, the faradic efficiency for formic acid is 77.4%, and the current density is  $4.8mA/cm$  at  $-1.09V vs RHE$  with an electrolyte  $0.1M KHCO_3$  [55]. Its active area is quite similar to this of tin metal, and this is because the remaining tin oxide is very thin.
- In the second case, to increase the formic acid production and current density, the electrode preparation technique needs to change. Anodized tin dioxide is removed from its substrate. It is mixed with acetylene carbon black, Nafion solution and isopropanol. The solution is sonicated and mixed until it becomes uniform, and then it is deposited on a carbon paper sheet. The tin dioxide has porous morphology, which is not altered by the electrode preparation, nor filled by the carbon powder. It has a huge Electrochemical Active Surface Area (ECSA)  $64.3m^2/g$ , it is very different from the previous case and also the current density is higher. Its best performance for  $CO_2RR$  is of 95% with a geometric current density of  $15.5mA/cm$  at  $1.06V vs RHE$  with the same electrolyte condition [28].

It is important to point out that the tin oxide preparation method has a big importance on the final properties of the electrodes. The anodized  $SnO_2$  ( $AOSnO_2$ ) has an advantage comparing to the commercial tin dioxide powder. This last has bigger nanoparticles and a smaller active area. An electrode prepared with the same components, but using a commercial tin dioxide powder has similar performances to the  $AOSnO_2$  at a small negative potential. At high negative potential, its faradic efficiency is reduced by mass diffusion limit effect. At  $-1.15V vs RHE$  the current density is  $7mA/cm$  and the faradic efficiency towards  $HCOOH$

is 43% [28].

### 3.3 Cycling Voltammetry

Cycling Voltammetry (CV) measurement is used to determine the active potential ranges of the working electrode and to investigate the range in which the material reduction and oxidation or other electrochemical reactions take place.

The technique is based on the potential variation with a determined rate of variation; it is the scan rate. It determines the width of the diffusion layer, and faster is the scan rate and smaller is the Helmholtz's layer, so the current increase [52].

The measurement usually takes place in a single cell with three electrodes dipped in a  $KHCO_3$  electrolyte. They are the working electrode, the  $SnO_2$ -catalyst, a counter electrode made by a platinum wire and a reference electrode, in this case it is  $Ag/AgCl$  with an electrolyte solution  $3M NaCl$ . To understand the working electrode electrochemical activity, the material is usually tested in an electrolyte saturated by different gases. In the case under analysis they were nitrogen  $N_2$  and carbon dioxide  $CO_2$ .

In both cases the gas is bubbled for 30 minutes inside the electrolyte saturate it. If we use nitrogen, the working electrode can generate only hydrogen evolution. This reaction in an electrolyte  $0.1M KHCO_3$  shows an increase in the current at  $-0.79V vs RHE$ , which is related to the HER [50]. If the introduced gas is carbon dioxide, a different electrochemical reaction is possible; including the carbon dioxide conversion into value-added products, including  $CO$  and  $HCOOH$ .  $HCOOH$  is the target product of this thesis; it requires quite high applied potential. The two reactions are active in the same range, but increasing the applied potential the formic acid selectivity increase up to  $-1.19V vs RHE$  [50]. Over that value the  $CO_2RR$  selectivity of the electrode drastically decrease.

The carbon dioxide dissolution in the electrolyte generates a pH variation, for example for  $0.1M KHCO_3$  it moves the pH from  $8.9pH$  for electrolyte without the  $CO_2$  up to  $6.8pH$  for  $CO_2$  saturated electrolyte [56]. This happens because the  $CO_2$  in aqueous solution interacts with water and generates carbonic acid. This last releases one of its hydrogen atoms that acidify the solution. It causes a potential shift according to Nernst's equation 2.5. The reaction with different pH has a different intrinsic potential. There is a shift of  $0.12V$  between the saturated solution with nitrogen at  $8.9pH$  and the same

saturated with  $CO_2$  at 6.8pH [50] [56].

There are two different standards to plot the results of the CV, the **US** convention where the highest applied potential is at the left side and the lowest is at the right side. The potential decrease from the left side to the right side. The oxidation peaks have a negative current. Instead, the reduction peaks are positive. The other convention is the **IUPAC**; it is the **US** convention rotated by  $180^\circ$ . The reduction peaks have a negative current and the oxidation a positive one, the highest potential is on the right, and the lowest is on the left. The two conventions are shown in Figure 3.7.

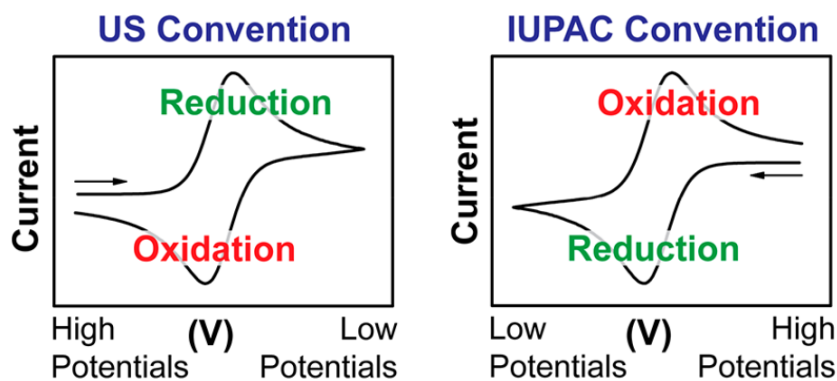


Figure 3.7: Cycling voltammetry convention [52].

In this thesis the **IUPAC** convention is adopted [52]. A typical range of analysis for a  $SnO_2$  catalyst is from 0 up to  $-1.8V vs AgCl/Ag$ , which is from  $0.61V$  to  $-1.19V vs RHE$ , and the range referred to the RHE was calculated using the Nernst's equation. Figure 3.8a and Figure 3.8b show typical cycling voltammeteries of a tin dioxide electrode, respectively based on  $SnO_2$  commercial and an anodized  $SnO_2$  annealed for 2 hours at  $450^\circ C$ .

In both the electrodes, the tin oxidation and reduction peaks are evident. The tin dioxide reduction and oxidation peaks are, the first between  $-0.5$  and  $-0.2V vs RHE$ , and the second between  $0.05$  and  $0.5V vs RHE$  [28]. In the case of both electrodes, an increase in the current with a potential more negative than  $-0.8V vs RHE$  is observed, and this is because at that value the HER and the  $CO_2RR$  start [50]. The electrode made of anodized tin shows a higher selectivity towards the  $CO_2RR$  then HER.

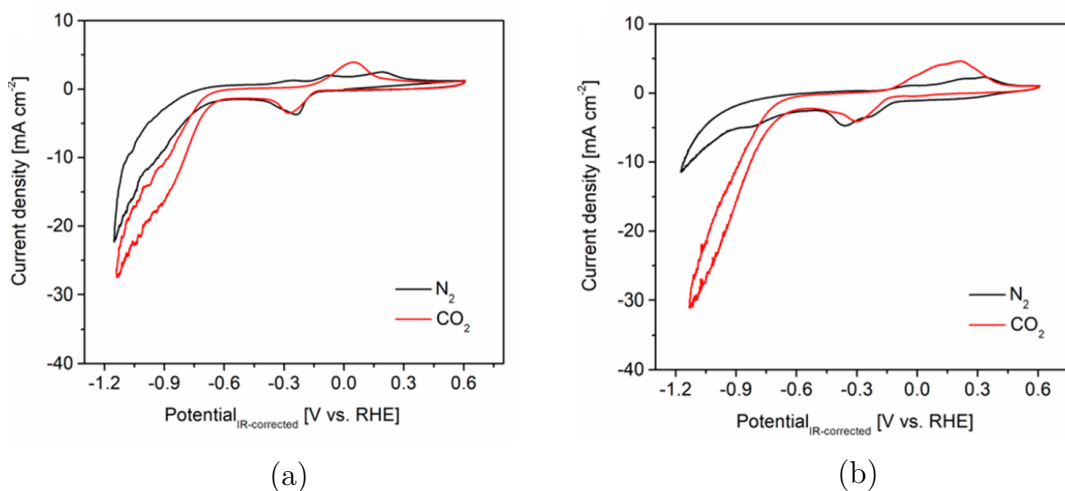


Figure 3.8: Cycling voltammetry of (a) commercial  $\text{SnO}_2$  and (b) anodized  $\text{SnO}_2$  [28].

## 3.4 Chromatographic analysis

The  $\text{CO}_2$  electrochemical reduction experiments result in the creation of gaseous or liquid products. The carbon dioxide reduction on a tin dioxide electrode generates carbon monoxide, hydrogen and formic acid. To quantitatively measure their concentration, chromatographic analysis is required. Formic acid is a liquid product which is analyzed by the High-Performance Liquid Analysis 3.4.1, the other two products are gaseous and are measured using the Gas Chromatography 3.4.2.

### 3.4.1 High Performance Liquid Analysis (HPLC)

HPLC is a chromatographic technique able to distinguish different liquid samples mixed in the same solution. This technology separates analytes according to their interaction with the surface of the column. It modifies the time required to reach the detector. The main component is the column, which is a packed hollow tube. The tube coating (static phase) creates a retention effect with the different analytes dissolved in the solution (mobile phase). Different fluids have a different interaction with the surface. This interaction determines their diffusion speed and it allows to separate the solutions according to their arrival time at the detector [57].

Different stationary phases are applied according to the analyzed solution

and the searched compound. Some examples are: the Adsorption Chromatography column that reacts with polar molecules and Reversed-Phase Chromatography where the apolar compounds are slowed. The diluent solution needs a small interaction with the stationary phase, and therefore has an opposite behaviour than the sample. Other retention mechanisms allow to separate charged molecules, particles with different sizes or molecules with a specific biological bond [57].

The detectors can be different according to the searched molecules. The most common is the UV-VIS characterized by a specific variation of light absorption, which depends on a specific class of compounds. It is mostly applied for acid detection. The detector response signal is used as a quantitative and qualitative measure. The measurement process can be seen in Figure 3.9.

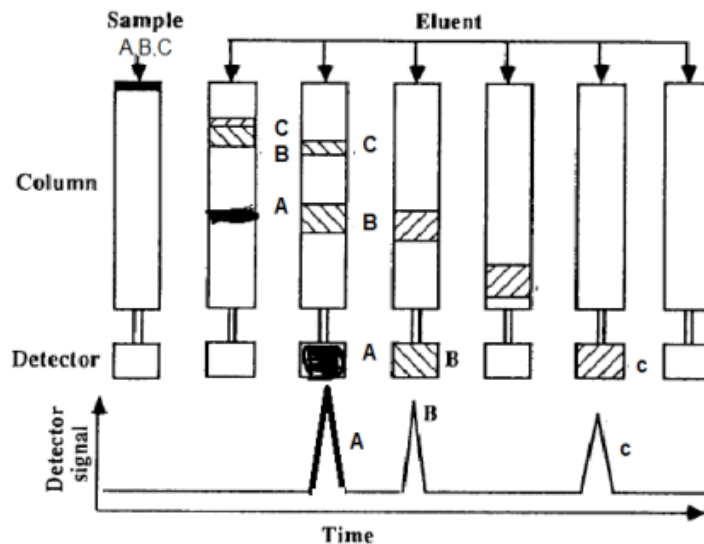


Figure 3.9: HPLC measure analysis [57].

The diluent solution has a small interaction with the static phase, after its detection, all other compounds will be detected at different time. Different arrival times mean different compounds, the shape and dimension of their peaks determine their concentration in the solution. The measurement is possible by comparing the data to the calibration curve.

HPLC is made of different components. The diluent solution is kept in a reservoir and then the sample is dissolved in it. Then the solution flow through a degasser that removes the gaseous molecules, which can alter the measurement. The solution is pumped in a high-pressure system that injects

the liquids in the pre-column. This last component is used to remove unwanted particles from the solution. Then it flows through the column, and the detector analyzes it [57].

### 3.4.2 Gas Chromatography (GC)

The gaseous products are analyzed using a GC. Similarly to HPLC, its main component is the column. It determines the interaction and the retention time for the gaseous molecules. The number of the detectable molecules depends on the column length and other geometrical factors [58]. Also, in this case, the sample is diluted in a mobile phase (an inert gas) that moves the gas solution through the column. Originally the columns were made of steel, but it was too reactive. Then these were covered with fused silica, they are known as a capillary column, which is the most widespread column technology. Nowadays also micro-GC is introduced, which is a smaller device, it can be portable but has some limitations in the number of detectable species. In this technology, the column is miniaturized like other components, and it is created usually etching a silicon wafer. The column geometry has an important role in its detection ability [58]. The internal column surface is coated with various materials depending on the analyzed molecule [59].

The gas speed is determined by the column temperature, pressure and wall retention time. Different gas phases will reach the column end with different time, so the analysis is very similar to the HPLC, shown in Figure 3.9.

The different arrival times are recorded using a detector. The most common type is the Thermal conductivity detector. This measures the gas concentration according to the temperature difference between a reference cell, filled with a pure carrier gas, and another cell where the gas solution flows through. The gas mixture generates a temperature variation that is recorded and compared to the calibration curve. It gives back information on gas typology and concentration. Other detectors exist and all of them compare a property variation of the gas solution with a reference case [58].

# Chapter 4

## Results and discussion on $SnO_2$ based electrode

In this chapter 4, there is the description of the synthesis and material characterization of  $SnO_2$  nanostructure obtained by anodic oxidation. It is followed by the description of  $SnO_2$  based electrode preparation and its electrochemical characterization. The focus is the electrodes preparation reproducibility. In brief, the preparation starts with anodic oxidation of the tin foil, which creates an oxide layer on the metal surface. This is then sonicated, to remove the grown layer from the substrate, and then annealed in order to obtain  $SnO_2$  crystalline structure. The obtained powder is used for the ink preparation, which is deposited on a carbon paper GDL to create an electrode, it is tested for the carbon dioxide reduction.

In addition to material and electrodes preparation and characterization, there is the description of the problems which have arisen and my solutions and how the process was modified to improve its efficiency.

### 4.1 $SnO_2$ synthesis and characterization

Tin oxide material preparation starts by tin anodic oxidation. The tin substrate is a foil ( $15 \times 15$ )cm with a thickness of 0.15cm, and a purity of 99.7%, made by Goodfellow. The substrates for anodic oxidation are obtained by cutting the foil in smaller portions, these will be the anodes. I decide that the optimal dimension to reduce waste material and to have a good oxide growth is ( $2.5 \times 2$ )cm. The cathode is a platinum foil of the same dimension, which is reused every time. All electrodes are ultrasonically cleaned for

twenty minutes with acetone at first and then with ethanol. Subsequently, they are dried with a nitrogen flow. These processes remove powder and other organic impurities that might have been there previously or were deposited over its surface during the cutting process.

The anodic oxidation process is described in section 2.1 and here there are the details of the experimental procedure only. The process is performed in a baker, filled with the electrolyte solution of  $0.3\text{M NaOH}$  in  $\text{H}_2\text{O}$ , under continuous stirring process. The electrodes are partially immersed in it, and it is important to pay attention not to wet the electrical contacts. These are crocodile clips that provide the necessary voltage of  $10\text{V}$  generated by the power supply (GWINSTEK SPD-3606). The synthesis lasts 30 minutes, which results in a quite thick oxide growth, and therefore a large quantity of the material is prepared. After the anodic oxidation, the tin foil covered with the oxide layer was rinsed in distilled water to remove the residual electrolyte. Figure 4.1 shows the set-up that have been used.

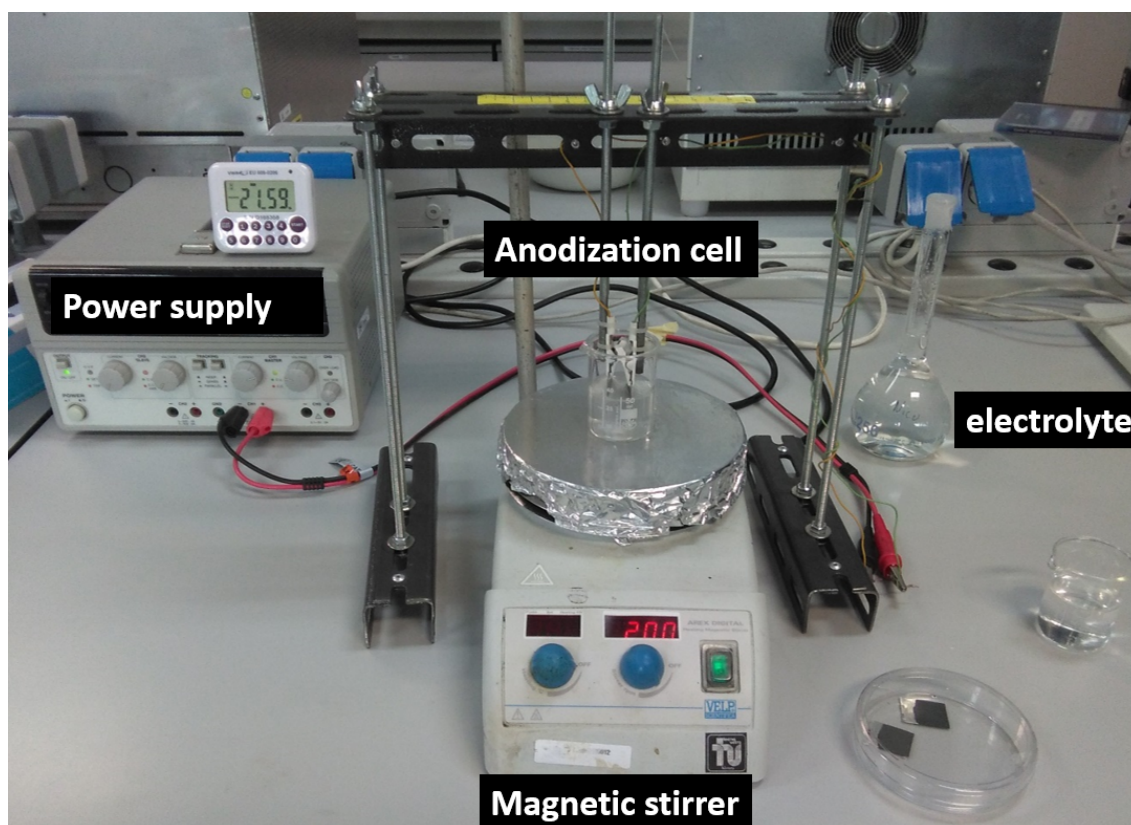


Figure 4.1: Anodization set-up

To prepare another sample, the solution is changed, and all the components

(backer, anodized tin foil, platinum foil) are washed using bi-distilled water. At this point, the process is restarted using a new solution. At the end of the anodic oxidation process the tin oxide layer has a brown/black colour. This is because the oxide layer is composed of a mixture of oxides with different oxidation state, the predominant is  $\text{SnO}$ , which has this colour. The oxide growth occurs only there, where the substrate is immersed, which is almost 3/4 of the whole area, as shown in Figure 4.2a.

FESEM was used to analyze the morphology of the as-grown material, it is shown in Figure 4.2b. The surface of the as-grown material is irregular, and some fragments are partially detached from it. It is the consequence of the oxygen bubbles evolution generated during the anodization process. The Figure (4.2c and 4.2d) studies the nanostructured morphology using an higher magnification.

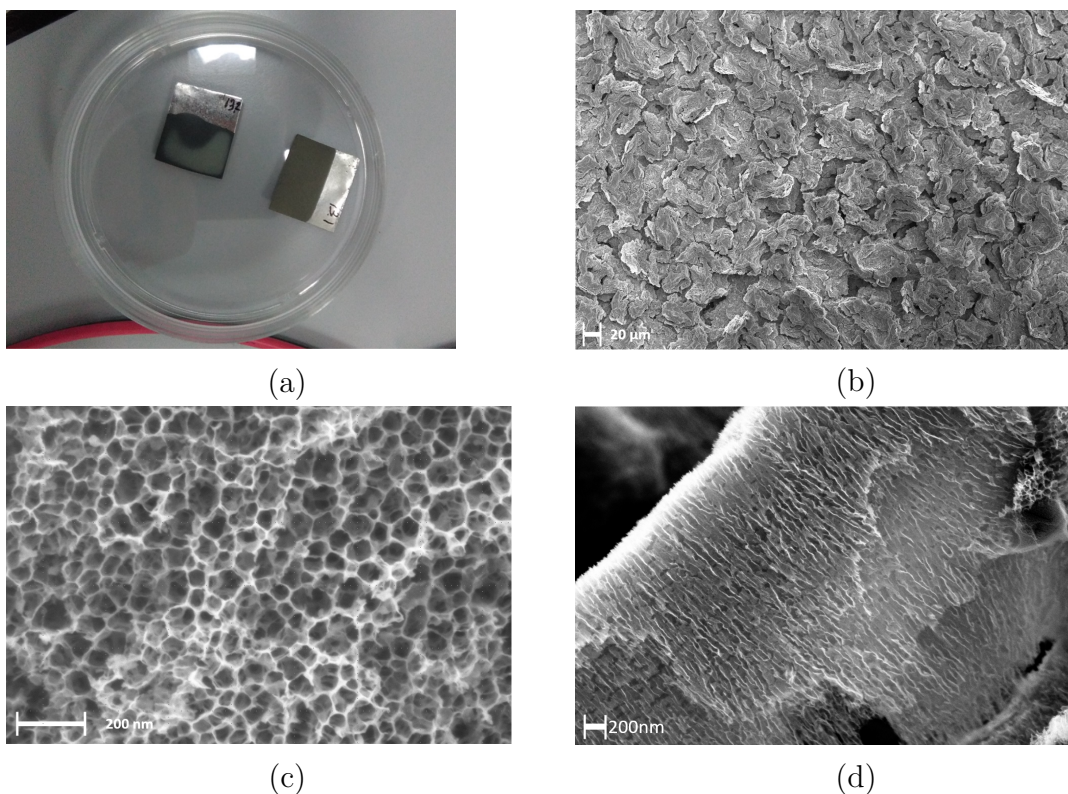


Figure 4.2: (a) Tin anodized samples; (b) and (c) FESEM images of the nanostructured surface samples with different magnification. (d) FESEM analysis of sample cross section.

Figure 4.2c shows a porous structure. The pores have very thin walls and a

non-regular structure, as described in section 2.1. Pores have various diameters, their average diameter is of about  $25\text{nm}$ , which is in agreement with previous results [28]. The cross-section view, presented in Figure 4.2d, shows that nanochannels are oriented along the growth direction. They are not continuous and well defined, but they are a combination of irregular pores that might bifurcate their self and after recombine. In addition, the oxygen bubbles might generate many micro-cracks perpendiculars to the growth direction. This is due to the formation of the bubbles during the anodic oxidation process, which interrupt the continuous growth.

I noticed that some events might deteriorate the oxide growth. The reaction generates oxygen bubbles, if one or more of them remain partially adsorbed on the electrode surface and enlarge their dimension, they might interact with the electrical contact. If this happens, an alternative electrical path appears and it reduces the oxidation growth. Another problem that can appear is if the process works with a current higher than the expected one. This could happen when the distance between the anode and the cathode is decreased too much. In this case, it might happen that the oxide layer, which grows quicker, is too thick and its adhesion to the substrate decreases. Therefore, the oxide layer peels off in small fragments and disperse in the solution. As a result, even if the current is higher the amount of oxide grown is drastically decreased.

At the end of one anodic oxidation round (including several growths), the platinum foil has an unwanted layer deposited on its surface. It drastically reduces the conductivity, therefore needs to be removed. To remove it, the electrode is rapidly dipped in an aqua-regia solution, and immediately washed many times in bi-distilled water. The aqua-regia solution is a mixture of hydrochloric acid and nitric acid, the composition is usually 2:1 or 3:1. It can dissolve the platinum itself, so the cleaning immersion to remove the external layer must be very fast to dissolve as little as possible the metallic foil [60].

## 4.2 Preparation of Tin oxide catalyst

### 4.2.1 Tin oxide removal from the metallic tin substrate

To create the electrodes, the oxide layer is removed from the substrate using a sonication process. Anodized tin foil are deposited in a backer filled with ethanol. It is placed in a sonicator (Elmasonic-P60H) and sonicated for more than one hour with a frequency of  $37\text{kHz}$  and sometimes they are manually

agitated.

The sonication breaks the tin oxide layer in fragments with different sizes. When the tin oxide layer is completely removed from the metallic substrate, the anodes are washed with ethanol to collect the fragments that are still attached to the substrates. During this process a suspension rich of tin oxide fragments in ethanol is created. In order to investigate the dimensions of the fragments, a FESEM characterisation was performed. For this test, a drop of the ethanol and tin oxide suspension is spotted on a holey carbon grid and left to dry. FESEM image in Figure 4.3 shows the range of the dimensions of the fragments, some of them could have a dimension of tens of micrometre. These last preserve the porous structure grown during the anodization process.

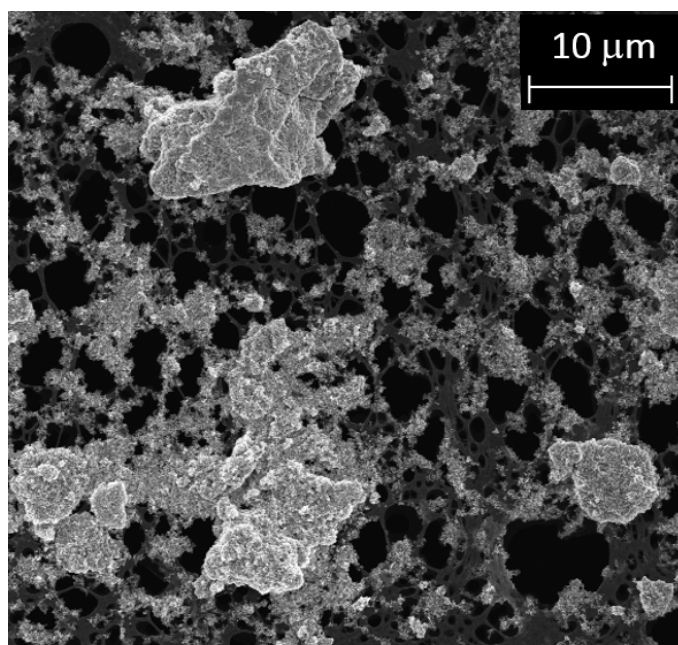


Figure 4.3: Tin dioxide fragments on a holey carbon support

In the next step, the tin oxide must be separated from the solvent. The ethanol suspension with the dispersed tin oxide is filtered using a nylon membrane filter (Durapore GVWP04700, made by Merck) with pores diameter of  $0.22\mu m$ . A funnel hosts the filter, and it is placed on the neck of a vacuum-flask. This is connected to a vacuum pump to improve the ethanol diffusion speed through the filter. The suspension is deposited over it, drop by drop. Then the filter is rinsed, and the tin oxide accumulated on it is removed and stored.

The process was optimized to perform quicker separation of the tin oxide from the solvent. The suspension is placed in falcons with equal volume and weight, then they are centrifuged (Eppendorf centrifuge 5804). The process parameters are 20 minutes at  $4200\text{rpm}/\text{min}$ . It creates a bottom body, that is removed and accumulated in a crucible, while the separated exhausted ethanol repeats the separation process. The liquid fraction repeats the centrifugation process until there is no more bottom body. The crucible filled with wet tin oxide fragments is left under the chemical hood to remove the residual solvent. This process guarantees a faster extraction of the solid component in a big suspension volume. It also holds particles smaller than  $200\text{nm}$  that would be lost during the filtration. In addition, it reduces the tin oxide movements from one element to another, decreasing the risk to lose the powder by an accidental error.

Some variations to the experiments were applied in order to obtain smaller and uniform in size fragments of tin oxide. This is because the obtained fragments are relatively large. Therefore the uniform distribution and mixture of the  $\text{SnO}_2$  with other electrode ingredients is easier when the size is decreased.

The first variation was the application of a periodic signal during the anodization process. With the idea to create pores with a specific thickness, and then the growth interrupt, which might favour the oxide broken. This is because the porous depth usually are very long (as shown in Figure 4.2d), resulting often in large fragments (as shown in Figure 4.3).

Hua Cheng and coworkers have shown that changing the applied potential during the growth results in a variation of the periodic structure, growth rate and pore diameters [30]. From this input, it was presumed that the introduction of the periodic potential might introduce the growth interruptions. In detail, at the positive potential, the structure growth proceeds as normal, and at the negative applied potential the growth stops.

The experiment was performed as follows, the anodic oxidation applied a periodic signal with a half period with a positive potential of  $10\text{V}$  and the negative potential of  $-0.5\text{V}$ . The half-period is 15s and 6s for sample 15.1 and 15.2 respectively. To investigate the results of this type of growth, a FESEM investigation was performed in the cross-section, and it is shown in Figures 4.4.

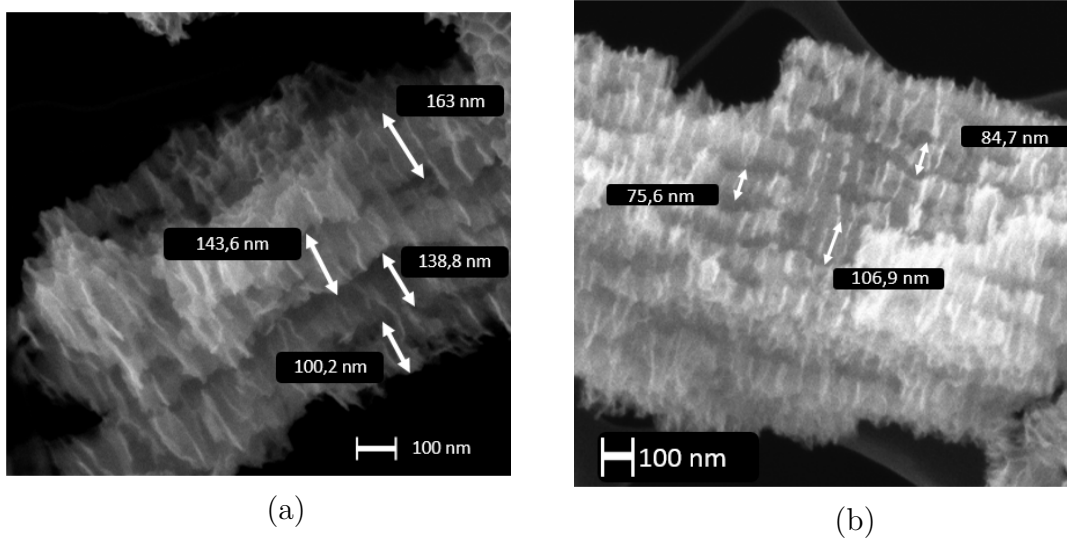


Figure 4.4: Pores depth analysis of samples: (a) 15.1 with a growth period of 15s and (b) 15.2 with a growth period of 6s.

These images (4.4a and 4.4b) show the depth of the pores for both samples and shows that in the case of the sample anodised at the period of 6s, the depth of the pores is smaller in respect to that with the period of 15s. And therefore it is in agreement with the anodic oxidation time. In the first case, it ranges from 75nm to 107nm, in the other from 100nm to 163nm. The material is then removed from the substrate in the usual way. During the sonication, the tin oxide layer breaks in fragments. However, their thickness is different from pores length of the layer grown in the half period; it brakes according to other fracture lines. The obtained fragments are more uniform, even if they still are a conglomeration of different pores sections. In any case, the process is long, and this drastically decreases production rate, therefore it was not used in the final experiments.

Another way to reduce the dimensions of the fragments is the manual grinding. Two samples (samples 17.8, 17.9) are manually ground for 10 minutes in an agate mortar, after the annealing treatment (which will be introduced in the following text). The grinding process reduces the size of the tin dioxide fragments, and it does not damage the porous structure as proven by the FESEM analysis.

### 4.2.2 Annealing

The annealing procedure is performed to improve the electrocatalytic performance [17], because the  $\text{SnO}_2$  has a better property than metallic tin or  $\text{SnO}$  [16]. The process working principles and characteristics are described in chapter 2.3. At this point of the process the tin oxide is a dark powder and it is collected in the crucible as shown in Figure 4.5a. The crucible is placed in the oven (Nabertherm LT 15/12/P330 muffle furnace) and annealed with a heating ramp of  $150^\circ\text{C}/\text{h}$  at room atmosphere for 2h at  $450^\circ\text{C}$ . At the end of this process, the sample cools down without any external action only by oven dissipation. Figure 4.5b shows the powder after the annealing procedure. It changes colour because the annealing favours the atoms reorganization and the introduction of oxygen, therefore the oxide is completely converted in  $\text{SnO}_2$  [42].

When the sample is at room temperature, it is removed and used to create the electrode for carbon dioxide reduction.



Figure 4.5: Tin oxide powder (a) before the annealing and (b) after it.

## 4.3 Electrodes preparation

The electrode preparation starts with the preparation of the suspension containing  $\text{SnO}_2$  in an eppendorf. Namely the elements are: tin dioxide powder  $10\text{mg}$ , acetylene black carbon  $1.5\text{mg}$ , Nafion 117 solution  $90\mu\text{L}$  and isopropyl alcohol  $320\mu\text{L}$ . The eppendorf is sonicated for 30 minutes to obtain a uniformly distributed suspension. This suspension will be deposited over a carbon paper gas diffusion layer. In the meanwhile, this last is cut to create the

electrode substrate with the dimension of  $(2 \times 2)cm$ . A tape with dimension  $(2 \times 0.5)cm$  masks one electrode side, thus it reduces the electrode surface to  $(1.5 \times 2)cm$ . The solution is deposited drop by drop over the unmasked electrode surface. The drops are poured until the surface is completely covered. The isopropyl alcohol naturally evaporates and the deposited layer becomes more compact. Meanwhile, the remaining dispersion is sonicated to be uniformly dispersed for the next deposition round. When the electrode surface has lost the majority of its liquid component, but it is still wet, the next layer is deposited. These processes is repeated until the dispersion finishes, at the end the catalyst has a loading of  $3mg/cm^2$ . The electrode is dried at room condition to remove the solvents. Figure 4.6a, obtained using a FESEM, shows the electrode surface. It is almost uniform and shows the presence of some cracks, which appear during the electrode drying process. The deposited active material is well connected to the electrode substrate, and the cracks do not influence the electrode structural strength, as they appear only in the top layers and don't propagate to the bottom layers and GDL. Figure 4.6b is a higher magnification, where are evident the electrode's components like the  $SnO_2$  porous structure and acetylene black carbon, this last has got a spherical shape.

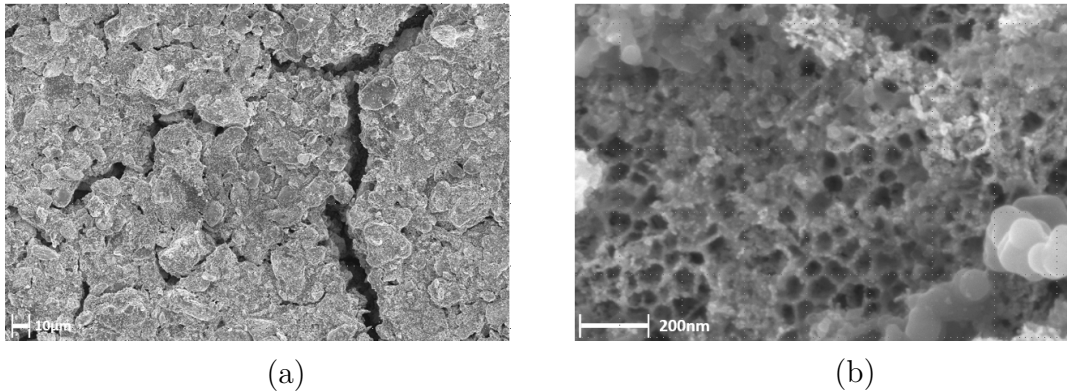


Figure 4.6: Top view FESEM images of an  $SnO_2$ -based electrode: (a) low magnification and (b) higher magnification.

The electrode is cut perpendicularly to the tape mask in the middle, therefore now there are two electrodes with an active area of  $(1 \times 1.5)cm$ .

We chose one of them; the tape mask is removed and in the free area, a conductive copper tape is positioned, then a new Kapton tape mask is set as the previous one, above the bottom of the copper tape. The same tape is used to cover also the back electrode. Its task is to inactivate the electrode

surface outside of the deposited active material.

## 4.4 Electrochemical characterization

The electrode is prepared according to the described procedure, the electrode is used as a cathode in the electrochemical H-Cell set-up. The power supply is CHI760D, it provides the desired potential during the chrono-amperometric measurement. At first, the electrode is reduced for 20 minutes with an applied potential of  $-0.99V$  vs  $RHE$  in a solution of  $0.1M$   $KHCO_3$ , saturated with  $CO_2$ . During the measurements, carbon dioxide is continuously flushed into the electrolyte. At the end, the solution is changed.

Similar electrodes have been already studied by the IIT research group. This work was performed to optimize the electrode fabrication procedures and make sure that the preparation results in reproducible electrodes. With this in mind, during the electrochemical characterization of these electrodes, the focus is the formic acid production. The samples are studied for 20 minutes with a chrono-amperometric measurement at  $-0.99V$  vs  $RHE$  and  $-1.19V$  vs  $RHE$ , which are the two most active potentials, and they were chosen based on the results from previous work on similar electrodes [28].

The reference electrode is an  $Ag/AgCl$  ( $3M$   $NaCl$ ), and during the measurements, it is set near the cathode. The anode is a platinum wire positioned in the other cell. After the measurement the electrolyte is extracted from the cathode chamber and it is analyzed using the HPLC, which provides the concentration of formic acid in the solution. Its concentration and the average current density gives the possibility to evaluate the samples' Faradic efficiency.

A number of electrodes were prepared to perform the electrochemical test and study the repeatability of the electrodes preparation procedure. These samples were obtained from the same tin dioxide batch and made following the previously described steps. The table 4.1 reports the electrodes faradic efficiency and their average current density ( $\vec{j}$ ). Five electrodes were produced in the way previously explained, and in the case of two electrodes (17.8 and 17.9), the tin dioxide was manually ground.

	$FE_{HCOOH}[\%]$	$\vec{j}[\text{mA}/\text{cm}^2]$	$FE_{HCOOH}[\%]$	$\vec{j}[\text{mA}/\text{cm}^2]$
	$-0.99V$		$-1.19V$	
17.1	58.0	5.5	63.1	7.1
17.3	55.4	3.9	65.1	7.1
17.4	69.1	7.8	57.6	9.8
17.6	71.3	7.1	59.8	8.4
17.7	55.8	5.7	71.2	9.2
17.8	80.6	5.5	73.1	8.3
17.9	72.3	5.5	79.4	8.0

Table 4.1: Comparison of the electrochemical results, the potential is shown vs RHE.

The samples preparation has a strong impact on the electrode performances. It might happen among various issues that the coating layer detaches from the electrode surface during the reduction. The results are summarized in Figures 4.7

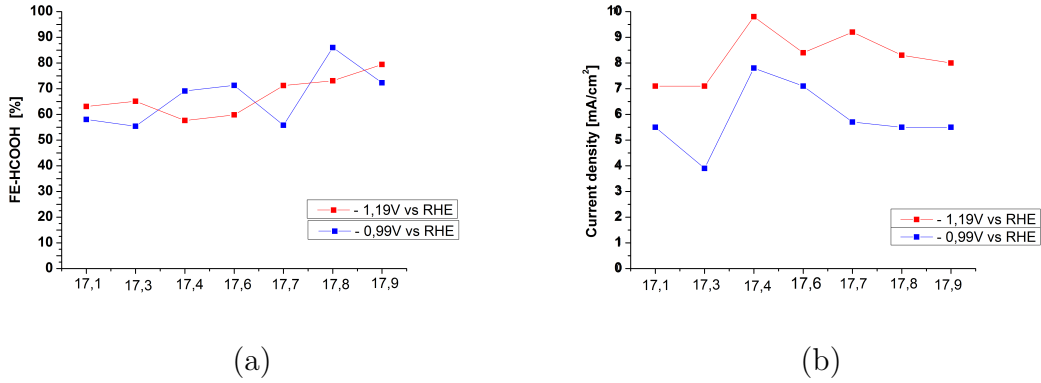


Figure 4.7: Electrodes results: (a) Faradic efficiency and (b) average density current [mA/cm<sup>2</sup>]

Figure 4.7a shows the comparison of the Faradic efficiency (FE) towards  $HCOOH$ , instead Figure 4.7b shows the average current density for all these samples, measured at both investigated potentials. It can be observed that for all samples, the average current density increases at more negative potential applied, which is expected. FE is quite stable, for some electrodes it is higher at more negative potentials and for others lower. In general, it is observed that the performance increases from sample to sample. In the first

five cases, the faradic efficiency is between (55 – 71.3)% at both potentials. According to the similar work performed in our group, we expect an increasing performance at  $-1.19V$  vs  $RHE$ . However, in some cases, this increase in performance at lower potential is not observed. The selectivity may be slightly different in the present case. This could also be related to the carbon dioxide mass diffusion limits or the problem with not sufficient  $\text{CO}_2$  dissolution in the electrolyte. In the last case, it could happen that during the reaction, the electrolyte condition changes, therefore the dissolved carbon dioxide concentration changes too. It means that at higher potential and higher current the reagents are consumed faster, the lack of  $\text{CO}_2$  obviously reduces its conversion possibility and then favours the hydrogen evolution reaction (HER). This can not be determined as only liquid phase products are analyzed.

Also the current is comparable between all samples, it ranges from  $3.9\text{mA}/\text{cm}^2$  up to  $7.8\text{mA}/\text{cm}^2$  at  $-0.99V$  vs  $RHE$ . Decreasing the potential to  $-1.19V$  the current density increases, it is between  $7.1\text{mA}/\text{cm}^2$  and  $9.8\text{mA}/\text{cm}^2$ . As already observed the current is increasing at more negative potentials for all the samples.

The samples 17.8 and 17.9, in which tin dioxide was manually ground, show higher faradic efficiencies, it is between (70 – 80)%. These values are in line with the published results on the same material obtained in the IIT's lab. Also, both samples have a similar average current density. It means that the electrical properties of the electrode coating layer do not change during the grinding process, but the faradic efficiency increases, which could be related to better dispersion of the ink components. With these final results, we assume that I have developed a good competence in reproducing samples with an uncertainty of 10% of their performances. The electrodes performances are similar to a similar electrode prepared within our team [28].

## 4.5 Conclusions

In this chapter 4, I describe my initial thesis work. I have learnt how to anodic oxidize the tin foil, the effects of the different parameters involved by this chemical reaction, including current, electrodes distance, time and etc. This process creates a nanostructured oxide layer on the tin substrate. It has a porous structure created by oxygen evolution. During the samples preparation, I identified some issues and I have found some solutions to overcome them.

To remove the tin anodized oxide layer, the samples are sonicated, the oxide layer breaks in small fragments and they detach from the substrate. I also improve the method to collect the anodized tin fragments.

A different growth process using a positive and negative potential is tested to obtain a nanostructured porous layered structure, which should break along planes. The oxide breaks and creates more uniform fragments, but the breaking points are not the plane between the two growth process. The oxide growth process is too slow and there is not a substantial fragments size variation. In order to get more uniform tin dioxide fragments, these last are ground for ten minutes. This process does not modify the nanostructured morphology.

Subsequently, I learn how to deposit the electrode for the electrochemical reduction reaction. I prepare a set of the electrode the first three have worst faradic efficiency between 55.4% and 69.1%. The samples 17.6 and 17.7 have a better faradic efficiency towards the formic acid production, the best result is 71%, it is the consequence of a better deposition process. The last two electrodes (17.8 and 17.9) are created adding one step to the tin dioxide powder preparation. The tin dioxide fragments are ground, it improves the electrode uniformity and generates a higher faradic efficiency, around 80%. Some samples have a decreasing efficiency at the smaller applied potential, it is caused by electrode mass diffusion limitation. These samples set have similar properties with a 10% of the variation. They have almost uniform catalytic and selectivity properties.



## Chapter 5

# Results and discussion on modified $SnO_2$ based electrode

In this chapter 5, there is the description of the modification of tin dioxide catalyst by the introduction of doping to improve its electrochemical performances, including selectivity and productivity. The chosen doping elements are Zinc and Titanium [29], and this choice was discussed within the section on doping 2.2. The doping is introduced after the standard samples preparation, and the annealing is then performed at a higher temperature. Material characterization is performed to determine the effect of the doping, the samples are analyzed using a FESEM, EDX and XRD techniques. The electrocatalytic performance toward the  $CO_2RR$  was then tested and compared to the undoped  $SnO_2$ -based electrode. This includes cyclic voltammetry, chronoamperometry and the complete analysis of the products using a micro-GC for the gaseous fraction, carbon monoxide and hydrogen, as well as the formic acid concentration, which is measured by an HPLC.

## 5.1 $SnO_2$ doping and characterization

Four electrodes have been made and one electrode is created without the doping atoms insertion, it is a reference sample named "Reference". There are 3 samples where  $SnO_2$  was modified by doping, which was introduced using ALD, or impregnation. For this samples, the tin oxide is prepared in the same way as in the previous chapter, with the only difference that for ALD the growth time was shortened to 10 minutes. This variation comes from the ALD limited aspect ratio, which is 2000 : 1 [37]. In fact in order to obtain a conformal deposition, and by considering the average  $SnO_2$  pore size (25nm) [28], the thickness should be in the range of  $50\mu m$  calculated with the approximation that the pores are continuous along the thickness.

In the case under analysis, four deposition cycles of zinc oxide have been done. The sample has been named "Zn-ALD". The FESEM analysis evidence no variation to its morphology, after the ALD deposition.

In the second case, wet impregnation was used for Zn and Ti doping. The anodic oxidation process has a duration of 30 minutes, and therefore a thicker sample is obtained. The impregnation process is quite slow, the solution is continuously stirred and the oxide cracks favour the dopants diffusion inside the oxide structure.

In this case, the dopants are introduced using 10mg zinc acetate dihydrate diluted in bi-distillate water; to obtain a final solution volume of 40mL [61]. The anodized tin foil is soaked for 2 hours in the obtained solution with continuous stirring. In the end, there is an accumulation of zinc and zinc oxides on its surface; the sample is named "Zn-wet". In the other case 240 $\mu L$  of titanium isopropoxide is dissolved in 40mL of isopropyl alcohol, the sample is soaked in this solution for four hours [62]. As in the previous case, at the end of the process, titanium atoms and titanium oxides molecules are accumulated on the surface; the sample is named "Ti-Wet".

Both samples are vigorously washed in bi-distillated water at the end of the process, then a FESEM analysis investigates their surfaces. The porous structure does not suffer any modification by the interaction with the impregnation solution. Figures 5.1 show the surface of the doped samples by titanium and zinc.

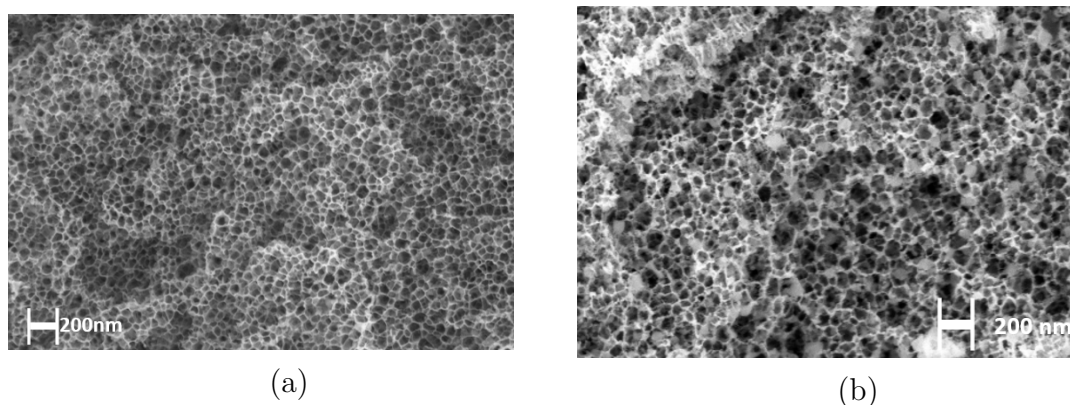


Figure 5.1: FESEM analysis of impregnated  $\text{SnO}_2$  samples: (a) Zn doping and (b) Ti doping.

During the doping, some structures and particles were created on the surface of the samples. These are rich in the doping elements. The impregnation procedures were optimised in order to reduce this effect. Using an EDX analysis in an area without these formations, the presence of doping atoms is detected. It suggests that the doping atoms dispersion is uniform. The EDX analysis confirms the presence of doping atoms in and over the tin oxide structures.

The impregnation is followed by annealing to both obtain the  $\text{SnO}_2$  crystalline structure and to promote the insertion of doping element in the structure. The samples placed on a copper foil and annealed with a heating ramp of  $150^\circ\text{C}/\text{h}$ , for 2 hours at  $370^\circ\text{C}$  without any pressure or atmosphere control. It favours the doping atoms reorganization inside the tin oxide crystal structure and a partial reorganization of the tin oxide crystalline structure and the conversion of  $\text{SnO}$  into  $\text{SnO}_2$ . Subsequently, the samples are sonicated to remove the oxide layer, in the same way as described in the chapter 4. Then, the tin oxide is annealed for four hours with an initial heating ramp of  $150^\circ\text{C}/\text{h}$ , at  $600^\circ\text{C}$  [63]. The two heating treatments progressively enlarge the tin dioxide particles size and deteriorate a bit the porous structure. It is a small modification, in fact, the structure keeps its morphology as confirmed by FESEM investigations. The effect of the annealing on the sample morphology, for one chosen sample, "Ti-wet", is shown in the images in Figure 5.2. The as-prepared and not annealed sample is shown in Figure 5.2a, and it shows the usual morphology of the as-prepared  $\text{SnO}_x$ . Figure 5.2b shows the morphology of the same sample after the annealing procedure.

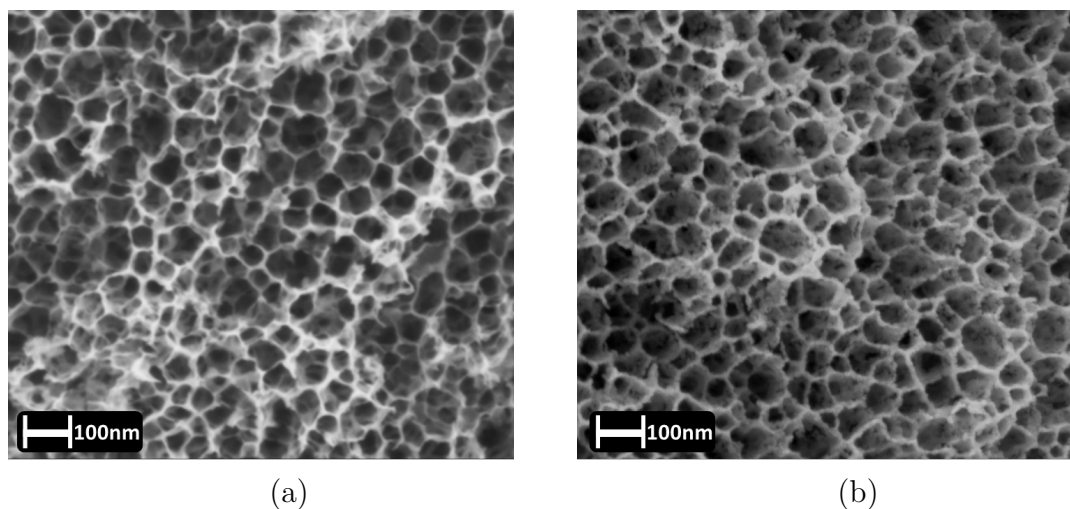


Figure 5.2: FESEM analysis of porous structure of the "Ti-Wet" sample: before(a), and after (b) the two heating treatments.

It is observed that the annealing enlarges the tin dioxide particles. During the annealing and reorganization of the structure a small deformation of the pores occurs, such as the formation of small holes inside the wall. In general, the enlargement of the particles could possibly decrease the mechanical structure properties and reduce the number of active sites.

### 5.1.1 EDX analysis

EDX analysis was performed to confirm the presence of the doping elements, and to have approximate information on the amount of deposited doping atoms in each configuration. The results of the quantitative measurement are shown, however it is important to keep in mind that the quantitative measurement with EDX is not precise if standards are not used. The exact quantity of the elements is not needed at this point.

This measure is performed on the doped  $\text{SnO}_2$  after the final annealing. The results are shown in table 5.1, where tin and doping atom atomic percentage is given. The accelerating voltage was  $15\text{kV}$ . This was measured on the as-prepared material, for all samples except the "Ti-Wet" sample. For the last the EDX was performed on the final electrode. During the electrodes preparation there are no chemical or physical treatments that might remove the doping atoms.

	Sn	Zn	Ti	$M_{Doping}/Sn[\%]$
ZnALD	19.3	2.9	-	15.2%
ZnWet	19.9	1.3	-	6.7%
TiWet	27.2	-	2.8	10.3%

Table 5.1: EDX analysis: atomic percentage of dopant and tin.

The analysis on the electrode also detects other atoms like fluorine contained in the Nafion solution and carbon atoms they are present in the black carbon acetylene and also in the Nafion solution. In all spectra, there is the presence of oxygen, which is an element of the tin oxide, and carbon. The following Figure 5.3 shows the spectra of "Zn-ALD" and "Zn-Wet" in powder and also "Ti-Wet" on the final electrode. Figure 5.3 and the table 5.1 confirm the introduction of the doping atoms into the samples.

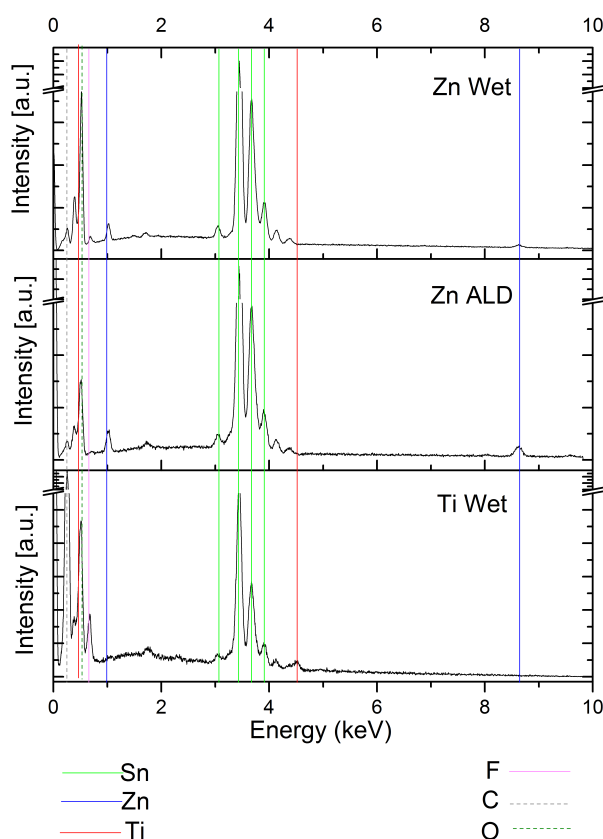


Figure 5.3: EDX spectra of the doped samples.

## 5.2 Electrodes preparation and characterization

The electrodes are deposited according to the description in the chapter 4.3. The FESEM analysis confirms that the electrodes are similar to the previous electrodes and the material is well dispersed.

### 5.2.1 XRD analysis

X-ray diffraction (XRD) patterns were acquired in a Bragg-Brentano mode to study the crystalline structures of final tin dioxide and try to detect the doping atoms effects. We decide to do this measure on the final electrodes because Nafion and black carbon do not alternate the measure in a significant way. In this way is also easier to analyze the  $\text{SnO}_2$  because it is inserted in a rigid an planar structure. Therefore the comparison with the doped electrode is easier. Figures 5.4 show the XRD spectra of the four samples.

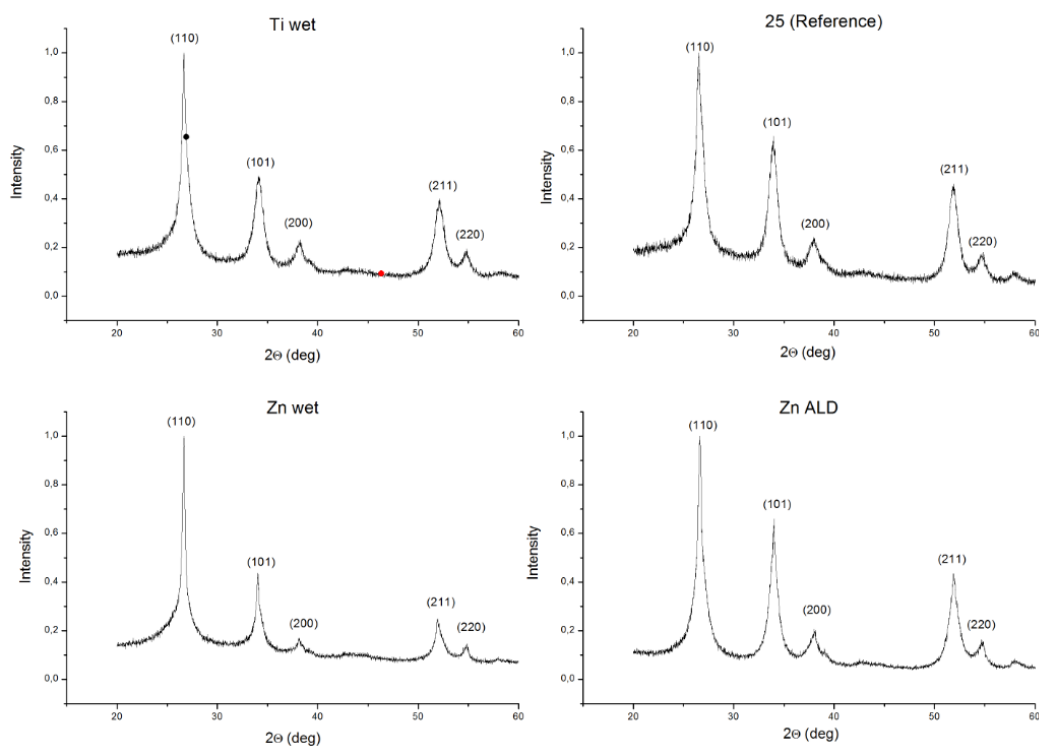


Figure 5.4: XRD spectra of: (a) "Ti-Wet", (b) "Reference", (c) "Zn-Wet", (d) "Zn-ALD". All spectra are normalized.

The XRD patterns of these electrodes display the main peaks for  $SnO_2$  (tin oxide JCPDS 00-041-1445) crystalline phase. The XRD spectra show only the  $SnO_2$  peaks, no additional contributions coming from secondary Zn or Ti metallic or oxide phases are detected, suggesting that most of the doping atoms are host in the  $SnO_2$  lattice structure. Tin dioxide crystal structure has many different orientations, it is a consequence of the disordered porous formation process. The pores wall are made of  $SnO_2$  crystalline nanoparticles organized in a chainlike structure.

As conclusion, the doping and annealing processes does not modify the porous structure. The EDX analysis confirms the presence of doping atoms, which are observed neither by FESEM nor by XRD analysis, suggesting that most of the doping atoms are host in the  $SnO_2$  lattice structure.

## 5.3 Electrochemical characterization

### 5.3.1 Cycling voltammetry

The electrocatalytic performance toward the  $CO_2RR$  of the  $SnO_2$ -based electrodes were first studied using cycling voltammetry (CV). This characterisation helps to evaluate the electrochemical active potential range for  $CO_2RR$ . The electrodes are prepared and protected in the same way described in the previous chapter 4.3. The only difference is the sample dimension, which is of  $(0.4 \times 0.5)cm$  with a whole area of  $0.2cm^2$ . The measurements are done in a single cell set-up, using three electrodes and under a continuous gas flow. The samples are tested in  $0.1M KHCO_3$  electrolyte saturated by  $CO_2$  or  $N_2$ . It is done distinguishing the different intrinsic electrolyte potential according to the different bubbled gas.

The potential range tested is from  $0.61V$  up to  $-1.2V vs RHE$ , with a scan rate of  $10mVs^{-1}$ . The electrodes have a similar trend compared to the examples reported in section 3.3, especially the reference electrode. In detail, in the "Reference" electrode, the tin oxidation and reduction peaks are evident. The tin dioxide reduction and oxidation peaks are from  $-0.5$  to  $-0.2V vs RHE$ , and from  $0.05$  to  $0.5V vs RHE$ , respectively. The current increases by a decreasing potential lower than  $-0.8V vs RHE$ . It happens because the HER and  $CO_2RR$  are favoured. The electrode made of anodized tin shows a higher selectivity towards the  $CO_2RR$  then HER.

The modified electrodes show some differences in the cycling voltammetry, because the doping atoms that are inserted in the tin lattice and/or create hetero-structures above the surface. In the first case, they might shift the

tin peaks, in the other, they might add their reduction and oxidation peaks. The doping atoms generate a small peak shape variation in the  $\text{SnO}_2$ .

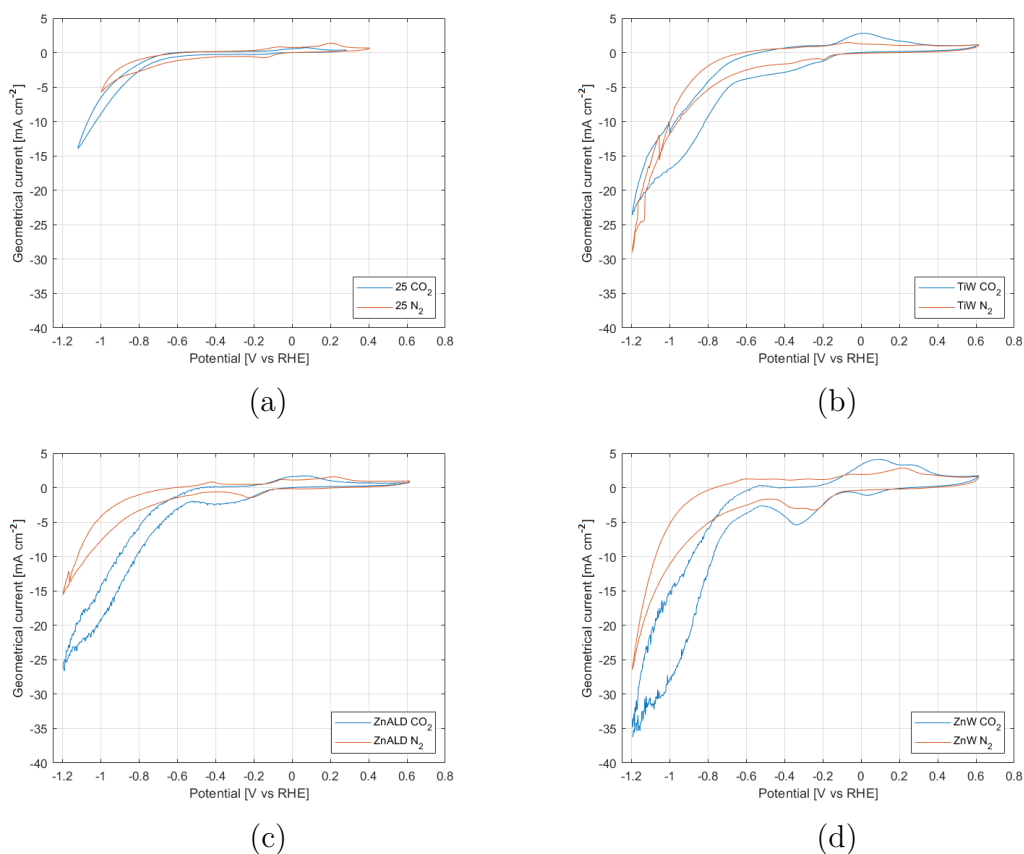


Figure 5.5: Cycling voltammetry for electrodes: (a) "Reference", (b) "Ti-Wet", (c) "Zn-ALD", (d) "Zn-Wet"

The cycling voltammetry measurements of electrodes prepared with doped tin dioxide show a similar trend to the electrode in which there is no doping. A higher current density is observed at the potentials more negative than  $-0.8V vs RHE$ . Higher current density is observed when the  $\text{CO}_2$  is bubbled to the electrolyte, than when the gas flow is  $\text{N}_2$ . This suggests that the electrodes are active for  $\text{CO}_2RR$ . The samples doped with zinc atoms in a different way have in increasing selectivity towards the  $\text{CO}_2RR$  at a potential between  $-0.5V vs RHE$  and  $-0.6V vs RHE$ .

### 5.3.2 Chronoamperometric Measurements

To compare the performance of the electrodes toward the  $CO_2RR$ , chronoamperometric (CA) measurements were carried out in an H-cell filled with (19 – 24)mL of 0.1M  $KHCO_3$  at different applied potentials. The solution volume depends on the height and the position of the electrode, the active area must be completely immersed in the solution. The cathode chamber is sealed with a silicone stopper. The set-up is shown in Figure 5.6. The mass flow (Bronkhorst EL-Flow Select F-201CV) strictly controls the carbon dioxide flow, which is 20mL/min, the gas bubbles at the bottom of the reaction chamber. The micro-GC (Inficon MicroGC F0G100) examines the ejected gas products concentration.

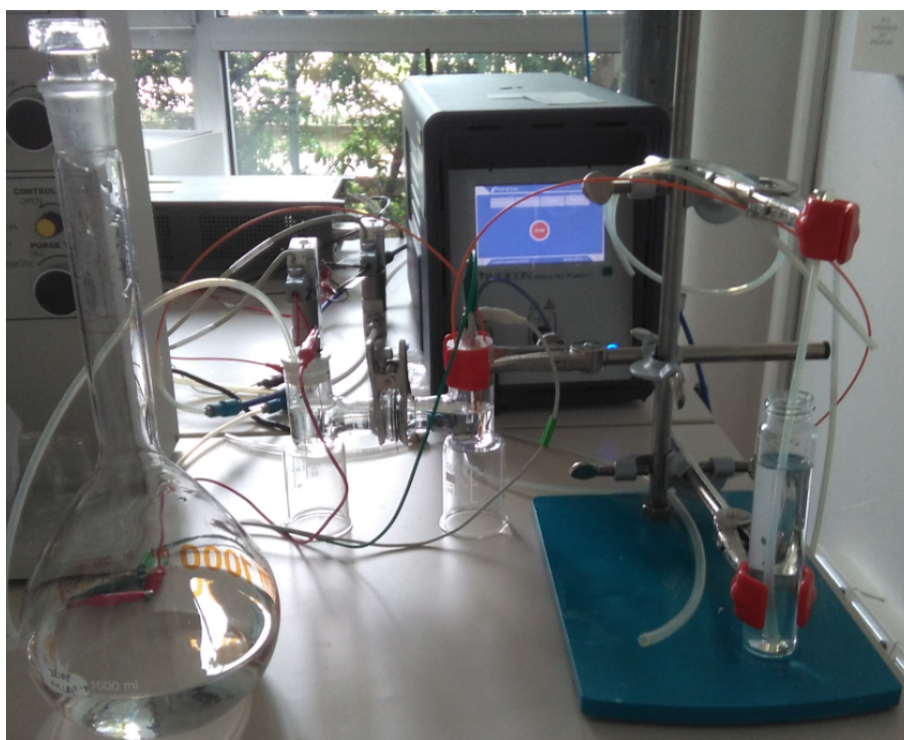


Figure 5.6: Electrochemical setup

Figure 5.6 has at its centre the H-cell, it is fixed using a laboratory support and a clamp. As described before the cathode chamber gas stream is strictly controlled and the gas chromatographer measures its composition, that is visible in the background. Each electrode is tested at four potentials, they are equally distributed between  $-1.2V$  and  $-0.59V$ , with a step of  $-0.2V$  between each tested potential. The applied potential is referred to the RHE,

as for all values reported in this chapter 5. The choice of the tested potentials was to have an overview of the catalytic activity and selectivity of the electrodes over the whole electrochemical range. Before testing the electrode at the first potential, it is pre-reduced at  $-0.99\text{V}$  for 20 minutes. The testing period changes according to the applied potential: at  $-0.59\text{V}$  it is  $1.5\text{h}$  or more, depending on the current. At all other potentials, the test time was  $1\text{h}$ . This difference is strictly related to the electrodes average density current and faradic efficiency towards formic acid. At  $-0.59\text{V}$  both are very low, and therefore to have at least  $5\text{ppm}$  of  $\text{HCOOH}$  in the solution (required by HPLC analysis) longer accumulation time is needed.

The test is performed at four potentials one after the other. A new solution is used at each potential. The solution with the product of the reduction reaction process is stored and measured with an HPLC.

The gas and liquid analysis allow us to measure the faradic efficiency of each product. The equation 3.5 is used to calculate the FE. It is the same equation as the one used in the previous chapter 4. In this chapter, both gaseous and liquid products are considered. The main difference to study their efficiency depends on how the volume is evaluated. In Figure 5.7, the faradic efficiencies of each product at every tested potential are reported.

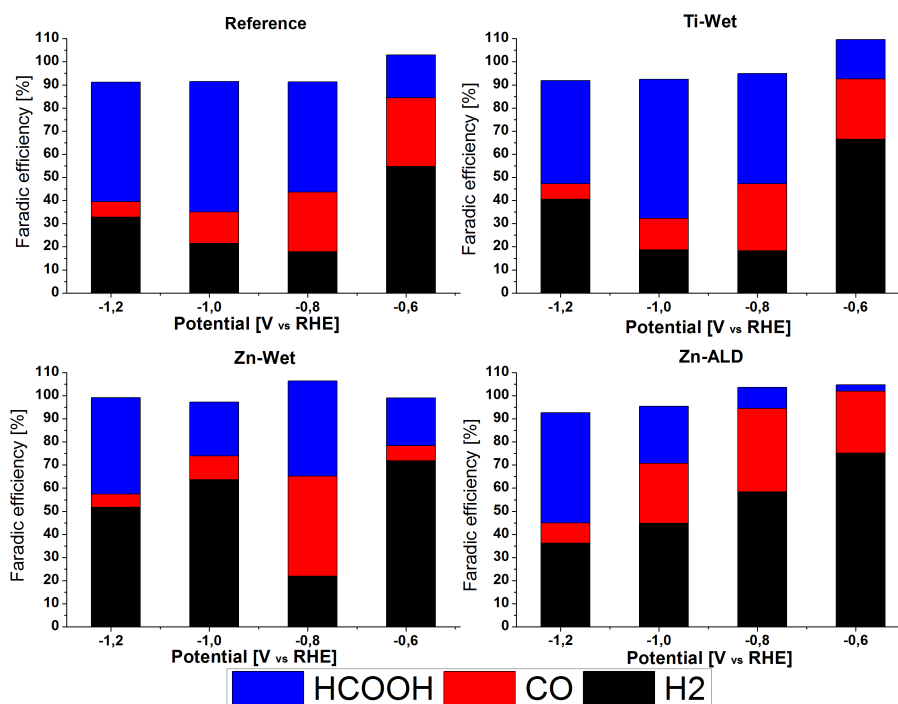


Figure 5.7: Faradaic efficiencies for  $CO$ ,  $HCOOH$ , and  $H_2$  formation on the electrodes at various potentials: "Reference", "TiWet", "ZnALD", "ZnWet"

During the experiment, the gaseous products are detected by a GC with the time interval of 3 minutes, while the formic acid concentration is studied by an HPLC at the end of the reaction.

The table 5.2 reports the faradic efficiency values for all products of all tested samples. The electrodes produce formic acid, carbon monoxide and hydrogen, they can be easily separated because the formic acid is liquid, instead the other two are gas.

The column  $FE_{TOT}\%$  is the sum of all the FE related to the different products, and it should have a value close to 100%. It might be a disagreement smaller than 10%. This happens because the FE equation 3.5 is strictly dependent on the transferred charge, which depends on the current. This last has some variations during the reaction, at the beginning, there is the reduction of the material and the Helmholtz's layer creation, so they drastically decrease the initial current to the working condition. In addition the bubbled gas at the bottom of the cell introduces a not negligible noise effect, that

directly acts on the current measured by the reference electrode. It might also happen that a bubble diffuses in the solution and stacks at the bottom of the reference electrode, this would induce a wrong reading.

Usually, the disagreement from 100% is related to the above discussed issues. In addition, the highest measured errors are observed at the highest potential (less negative). This is because the average current density is low, therefore the noise effect influences it strongly.

[V vs RHE]	$FE_{H_2}\%$	$FE_{CO_2}\%$	$FE_{HCOOH}\%$	$FE_{TOT}\%$
Reference				
-0.59V	54,7	29,7	18,5	102,8
-0.79V	17,9	25,7	47,7	91,4
-0.99V	21,5	13,5	56,5	91,5
-1.19V	32,8	6,6	51,7	91,2
Zn-ALD				
-0.59V	75,1	26,8	2,7	104,7
-0.79V	58,4	36,0	9,1	103,6
-0.99V	44,9	25,8	24,8	95,5
-1.19V	36,2	8,7	47,7	92,6
Zn-Wet				
-0.59V	71,8	6,6	20,6	99,0
-0.79V	22,0	43,2	41,2	106,4
-0.99V	63,6	10,3	23,3	97,2
-1.19V	51,8	5,6	41,7	99,1
Ti-Wet				
-0.59V	66,5	26,1	17,0	109,7
-0.79V	18,3	28,9	47,7	94,9
-0.99V	18,7	13,6	60,2	92,5
-1.19V	40,6	6,6	44,6	91,8

Table 5.2: Faradaic efficiencies for all products for all tested electrodes.

The "Reference" electrode shows an increase in selectivity to convert the carbon dioxide at more negative potentials. It is observed that the  $CO_2RR$  competes with the  $HER$  at potential smaller than  $-0.59V$ . The FE value for  $H_2$  evolution reduces from about 55% at  $0.59V$  to 18% at  $-0.79V$  and then increases again to reach 33% at  $-1.19V$ . The FE for  $CO$  production reduces from about 30% to about 7% in the tested potential range. The highest FE for  $CO_2RR$  of 73.4% is obtained at  $-0.79V$  (in this case the

total FE is of 91.4%). It is the combination of FE of 47.7% for formic acid and 25.7% for  $CO$ . The highest FE of 56.5% for  $HCOOH$  production is at  $-0.99V$ . Then it decreases slightly, however, the  $HCOOH$  production rate is higher at a more negative potential, as the total current is still increasing. The doped samples have a similar trend for HER, which is dominant at the lowest potential. However, the FE value for  $H_2$  evolution is higher. It is about 70% at  $-0.59V$ , decreasing the potential also HER decrease, it has a different trend for different samples. It is true for "Zn-ALD" it starts from 75.1% at  $-0.59V$  and it decreases at 36.2% at  $-1.19V$ , it oscillates for "Zn-Wet", in this case the HER starts at 71.8% at  $-0.59V$  and at smallest potential  $-1.19V$  it is 51.8%. The HER for "Ti-Wet" decreased to 18.3% and then increase again up to 40.6%.

The FE for  $CO$  production in doped samples shows the highest value at  $-0.79V$ , with the value of about 36%, 43% and 29% for "Zn-ALD", "Zn-Wet" and "Ti-Wet" respectively. The FE for  $CO$  than reduces to about 9%, 6% and 7% at  $-1.19V$  respectively. It is observed therefore than Zn doped samples show higher FE for  $CO$  than the "Reference" and "Ti-Wet" electrode.

The "Ti-Wet" sample have performances similar to the reference electrode at  $-0.79V$   $FE_{HCOOH}$  47.7% and  $FE_{CO}$  28.9% where the  $FE_{TOT}$  % 94.9%. At  $-0.99V$  there is the peak of formic acid production, that is 60% with a total efficiency of 92.5%. Also the mass diffusion limit is similar to the reference with a HER of  $FE_{H_2}$  40.6% with  $FE_{TOT}$  % 91.8%.

The "Zn-ALD" shows the worst selectivity for  $CO_2RR$ , and therefore also the highest contribution to HER. The best results are obtained at  $-1.19V$  with  $FE_{HCOOH}$  47.7% and  $FE_{CO}$  8.7%, with a  $FE_{TOT}$  % 92.6%.

The last sample is the "Zn-wet", and its most interesting potential is  $-0.79V$ , where the HER drastically decreases and the formic acid and carbon monoxide rapidly increase. At this value the faradic efficiency parameters are  $FE_{HCOOH}$  41.2% and  $FE_{CO}$  43.2% where the  $FE_{TOT}$  % 106.4%. However, relatively low current is observed at this potential, and therefore it is not the most valued one. This will be discussed in the following part, after the introduction of the currents at relative potentials.

The electrodes current ranges from a few hundred of microampere at higher potentials, up to about ten milliamperes at the lower ones. The literature suggest that the maximum current for H-cell set-up is  $35mA/cm^2$  [53]. The table 5.3 displays the electrodes measured average current density at a different applied potential.

	average density current [ $\text{mA}/\text{cm}^2$ ]			
	-0.59V	-0.79V	-0.99V	-1.19V
Reference	0.2	2.1	5.1	7.7
ZnALD	1.5	5.9	9.4	10.2
ZnWet	0.7	2.7	7.3	14.1
TiWet	1.0	2.7	6.3	9.5

Table 5.3: Electrodes average density current [ $\text{mA}/\text{cm}^2$ ] at different applied potential.

Obviously, at higher applied potentials (less negative), smaller current is observed. The reported values are expressed in [ $\text{mA}/\text{cm}^2$ ]. Doped samples have a higher current than the reference electrode. The "Zn-ALD" is the best in the range between  $-0.79\text{V}$  and  $-0.99\text{V}$ . The highest average current density is observed for "Zn-Wet" at  $-1.19\text{V}$ . Coming back to the productivity of this electrode, at this potential the FE for  $\text{CO}_2\text{RR}$  is not the highest. However, combining both high current and relatively good FE it still shows the highest productivity according to Figure 5.8b.

To summarize the obtained results Figures 5.8a show the faradic efficiency for  $\text{CO}_2\text{RR}$ , it is the sum of the  $\text{HCOOH}$  and  $\text{CO}$  contribution. Figure 5.8b shows the average current density devoted to the carbon dioxide catalysis.

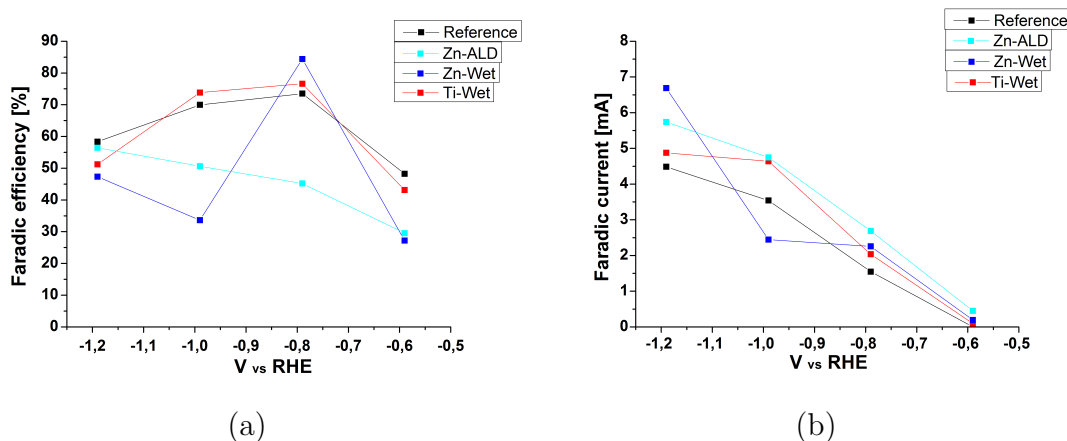


Figure 5.8:  $\text{CO}_2\text{RR}$  results: (a) Faradic efficiency ( $\text{HCOOH}\% + \text{CO}\%$ ) and (b) Average current density dedicated to the  $\text{CO}_2\text{RR}$ .

The doping increases the production rate of  $\text{HCOOH}$  and  $\text{CO}$  at lower potentials. The FE for  $\text{CO}_2\text{RR}$  is not increasing with more negative potentials,

but doping increases the average current density, and this is resulting in increased productivity.

The "Zn-Wet" has an optimal conversion performance at  $-0.79V$ . At the lowest potential,  $-1.19V$ , the mass diffusion limits reduced its performances, and the "Reference" electrode shows slightly better selectivity than the others. However, the "Reference" electrode shows a lower current at more negative potentials. And in general, the productivity for desired products is better. This also happens because it has a smaller current. The doped electrodes have a smaller selectivity towards the formic acid production. The productivity is usually better, even if faradic efficiencies are lower, as a consequence of higher average current density. This is true for all electrodes at each tested potential, except for the "Zn-Wet" at  $-0.99V$ . The zinc doping has better conduction. Their highest value is at  $-1.19V$  where the "Zn-Wet" has an average density current for  $CO_2RR$  of  $6.7mA/cm^2$ , the "Zn-ALD" value is  $5.7mA/cm^2$ , and it is  $4.5mA/cm^2$  for "Reference" sample.

## 5.4 Tested electrode characterization

After the electrochemical tests, the electrodes were investigated using a FE-SEM. The purpose of this was to observe, which modifications the catalyst undergoes during the electrochemical reaction. The electrode morphology of tested electrodes is shown in Figures 5.9. The analyzed electrodes are the same that have been observed before the electrochemical characterization.

The analysis of the top surface evidence that the electrode changed during the testing. There are large particles observed and this shows that the material has a tendency to recrystallize and/or agglomerate into larger particles, and the porous structure is not present at the top surface in these tested electrodes. In Figure 5.9a is evident the loss of the porous morphology. During the electrochemical reaction, the tin oxide particles are reduced under the applied potential during the electrons transfer to the  $CO_2$  and to the  $H_2O$ . The oxidation state changes and the average size changes. The particles changed visibly to larger, however as confirmed by IIT's previous research, the large observed particles are made of very small crystals. This can be only appreciated by TEM observation or XRD analysis [28].

In all doped electrodes, the final surface has changed, and at the end of the reduction reaction, all the samples lose the porous morphology on the surface. Figure 5.9b shows the "Ti-Wet" electrode, and large particles, some in the cube shape, are observed at the surface. Figure 5.9c shows the surface of the

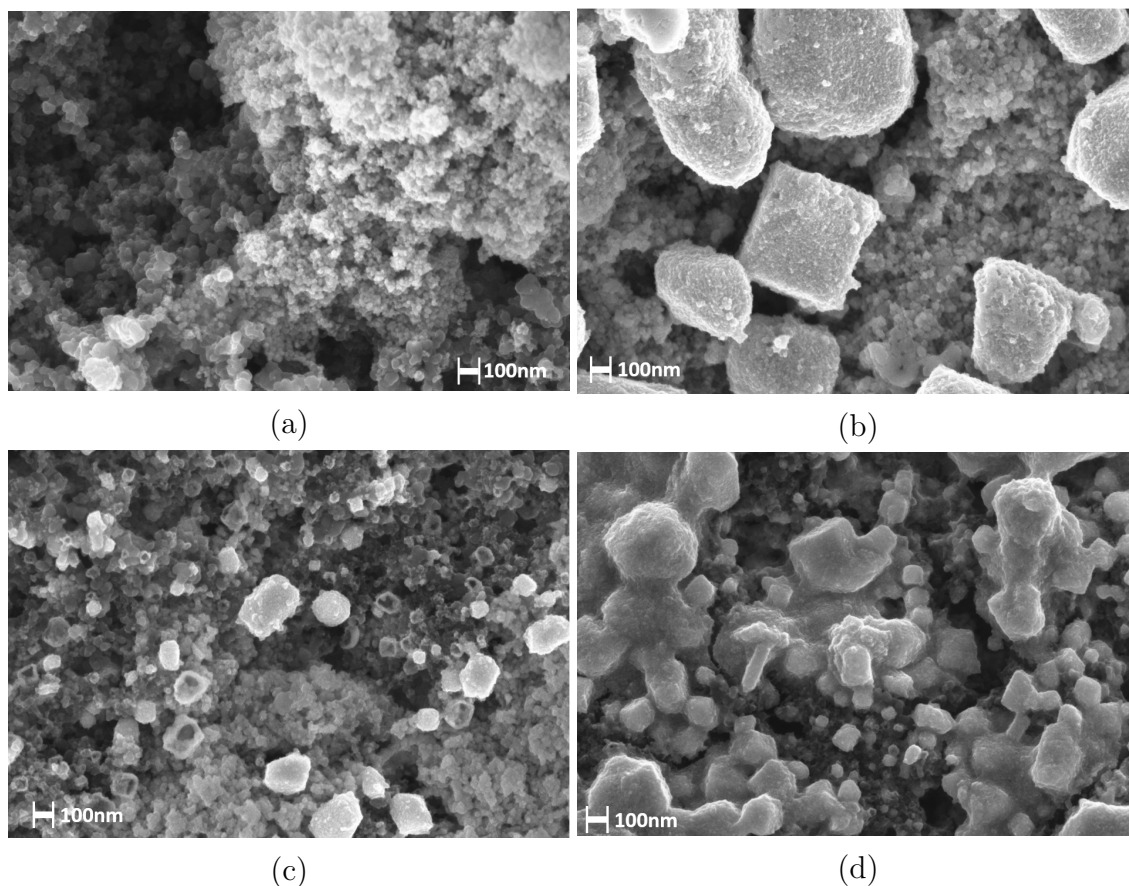


Figure 5.9: FESEM analysis of tested electrode surface: (a) Reference, (b) "Ti-Wet", (c) "Zn-ALD", (d) "Zn-Wet"

"Zn-ALD" and also in this case there is a lot of agglomerated tin oxide, these are less regular and smaller than in "Ti-Wet". The "Zn-Wet" morphology is drastically changed, like the other electrodes, it shows many agglomerates, and some have a quite regular shape.

## 5.5 Discussion on electrodes results

Starting from the idea of Karthikeyan Saravanan and co-workers, who suggest that doping of tin oxide with some elements including, zinc and titanium increases the electrodes  $\text{CO}_2\text{RR}$  performances [29], these selected doping element atoms are inserted in the samples. The doping atoms are inserted in the anodized tin structure, with the help of the Atomic Layer Deposition or the impregnation technique. To favour the doping atoms adhesion on the

surface or to promote their insertion in the tin oxide crystalline structure, the tin doped anodized samples are annealed on their native substrate at 370°C. After this heating treatment the oxide layer is removed from the substrate and the obtained powder is annealed at 600°C. There is no evident change in the morphology in the doped samples. The EDX analysis confirms the presence of doped atoms over or inside the tin anodized porous structure. The XRD analysis does not detect their presence in the form of metallic or oxide phases. This is the evidence that the doping atoms were inserted in the tin dioxide crystalline structure. In the next step the electrodes were prepared and the electrochemical characterization was performed. First cycling voltammetry was performed to study their electrochemical performances and understand if there is some variation of the overpotential for  $CO_2$  reduction. In general the doped electrodes have higher current. The zinc doping slightly shifts the active-potential position towards higher values, and therefore reduce the necessary overpotential, which is very desired and was predicted by Saravanan [29].

Then the electrodes are tested at four different potentials to evaluate the current density and faradic efficiency for each product for each of them. The doped electrodes have a higher average current density and improved productivity of  $CO_2RR$  products, they produce carbon monoxide and formic acid. These products have two different phases so they can be easily separated. In general, the doped samples have an increase in carbon monoxide production. The reduction of the electrodes' faradic efficiency at low potentials might be caused by the introduction of the doping element, or the surface modification and pores structure loss, which is caused by the tin dioxide reduction during the electrochemical reaction.



## Chapter 6

# Conclusions and perspectives

The climate changes are caused by the greenhouse effect that is strictly related to the increasing concentration of  $CO_2$  in the atmosphere. It is an emergent issue and electrochemical  $CO_2$  reduction with its conversion into a value added product is a promising technology to address this problem.

This thesis reports on  $SnO_2$ -based nanostructured electrodes for  $CO_2$  reduction reaction ( $CO_2RR$ ). The catalyst is prepared by anodic oxidation of metallic tin. The applied potential is 10V, and the electrolyte is a solution of  $H_2O$  and  $NaOH$  (0.3M). Nanostructured material with a porous morphology is obtained. The pores walls are composed by tin oxide particles that are crystallographically interconnected with a chain-like structure. The nanostructured layer is a mixture of  $SnO$  and  $SnO_2$ . It is removed from the substrate using a sonication process in an ethanol, resulting in fragments of  $SnO_x$  with sizes from some hundreds of nanometers to tens of micrometres. The catalyst detachment process is improved during the thesis; at the end, it is done by a centrifugation process, that separates the  $SnO_x$  fragments from the liquid fraction. They are annealed for 2 hours at 450°C, to improve the catalytic properties for  $CO_2RR$ . The tetragonal rutile crystalline structure is obtained ( $SnO_2$ ), and the morphology remains unchanged [28].

The  $SnO_2$  nanostructured fragments are mixed with acetylene carbon black, nafion solution and isopropyl alcohol, to create an ink. It is then deposited on a carbon paper gas diffusion layer, which creates an electrode for  $CO_2$  reduction. A number of electrodes was prepared in order to test their performances and to improve the ability to deposit uniform electrodes in reproducible way. In the second set of electrodes doping is introduced into  $SnO_2$  with the goal

to improve the catalyst properties, including the reduction of the overpotential for  $CO_2RR$ . The introduced doping atoms species are titanium and zinc, and they are inserted either by ALD or by wet impregnation. The impregnation methods were optimized and the dopants presence is confirmed by the EDX analysis. After this process, the samples are detached from the substrate and annealed at temperature up to  $600^\circ C$ . The temperature of annealing is higher than for undoped samples, and the reason for this was to favour the doping atoms insertion in the  $SnO_x$  lattice structure, in addition to transformation to rutile crystalline structure [63]. It also improves the crystallinity of its particles. The FESEM analysis confirms that the processes did not modify significantly the morphology. The catalyst and the electrodes are prepared in the same way as the undoped ones. XRD analysis evidences only  $SnO_2$  phase, and no additional contributions coming from secondary Zn or Ti metallic or oxide phases was observed.

The electrochemical characterisation shows that the doped samples have higher catalytic activity compared to the undoped reference electrode. Their  $CO$  production rate is increased, while the Faradaic efficiency (FE) for  $HCOOH$  is slightly lower. However, the overall productivity is higher, as a result of higher current density observed for all doped samples. In addition it is observed that the zinc doping seems to slightly shift the active potential towards higher values, and therefore reduce the necessary overpotential, which is very desired. This was the predicted behaviour by the literature [29].

The FESEM analysis of tested electrodes show that these samples have a substantial variation of their morphology.

Future work is linked with further characterisation of the presented structures and electrodes, in order to understand better the doping effect and durability of the electrodes. This includes X-ray Photoelectron Spectroscopy (XPS) analysis to investigate the doping effect, Electrochemical Impedance Spectroscopy (EIS) analysis to determine its electrical properties and a deeper structural and morphological characterisation in order to give some more insight to the modifications the catalysts undergo.

According to the future prospective and economical analysis the  $HCOOH$  is a very desired product and feasible to be obtained via electrochemical  $CO_2RR$ .  $SnO_2$  based catalysts are very promising for this application. However, in order to be applicable at industrial level, catalytic properties of  $SnO_2$  need to be further improved, and this includes both FE and current densities. In order to achieve this goal, for future work the variation of annealing temperature and its influence on the catalyst properties should be explored.

Subsequently more complex doping, e.g. co-doping should be tested. The

two doping elements would perform two tasks, one would be introduced to improve the catalytic properties, and another one to improve the conductivity. If this would be successful than the amount of carbon black, which contributes to the HER, could be reduced or completely eliminated, resulting in improved efficiency of  $CO_2RR$ .



# Bibliography

- [1] American Chemical, American Geophysical Union, and American Meteorological Society. October 21, 2009. 2009.
- [2] Effects | facts – climate change: Vital signs of the planet. <https://climate.nasa.gov/effects/>. (Accessed on 11/26/2019).
- [3] Causes | facts – climate change: Vital signs of the planet. <https://climate.nasa.gov/causes/>. (Accessed on 11/26/2019).
- [4] Carbon dioxide | vital signs – climate change: Vital signs of the planet. <https://climate.nasa.gov/vital-signs/carbon-dioxide/>. (Accessed on 11/26/2019).
- [5] Climate change: Atmospheric carbon dioxide | noaa climate.gov. <https://www.climate.gov/news-features/understanding-climate/climate-change-atmospheric-carbon-dioxide>. (Accessed on 11/26/2019).
- [6] International Energy Agency. Key world energy statistics. 2017.
- [7] Executive Summary. World Energy Outlook. 2017.
- [8] BP Energy Outlook 2019 edition The Energy Outlook explores the forces shaping the global energy transition out to 2040 and the key uncertainties surrounding that. 2019.
- [9] Carbon capture, utilisation and storage - fuels & technologies - iea. <https://www.iea.org/fuels-and-technologies/carbon-capture-utilisation-and-storage>. (Accessed on 12/05/2019).
- [10] Exploring Innovation Pathways. World Energy Scenarios 2019. 2019.
- [11] Matthew Jouny, Wesley Luc, and Feng Jiao. General Techno-Economic Analysis of CO<sub>2</sub> Electrolysis Systems. 2018.
- [12] Review of Technologies for Gasification of Biomass and Wastes Final report. (June), 2009.
- [13] Bio Sng and Feasibility Study. Bio-SNG.
- [14] Review of Technologies for Gasification of Biomass and Wastes Final

- report. (June), 2009.
- [15] Igor Yuranov, Nordahl Autissier, Katerina Sordakis, Andrew Dalebrook, Vit Orava, Peter Cendula, Lorenz Gubler, and Gabor Laurenczy. Heterogeneous catalytic reactor for hydrogen production from formic acid and its use in polymer electrolyte fuel cells Heterogeneous catalytic reactor for hydrogen production from formic acid and its use in polymer electrolyte fuel cells. 2018.
- [16] Chan Woo Lee, Heon Cho, Dong Yang, and Ki Tae. Reaction Mechanisms of the Electrochemical Conversion of Carbon Dioxide to Formic Acid on Tin Oxide Electrodes. pages 2130–2136, 2017.
- [17] James E Pander, Dan Ren, Yun Huang, Wei Xian, and Samantha Hui. Understanding the Heterogeneous Electrocatalytic Reduction of Carbon Dioxide on Oxide-Derived Catalysts. pages 219–237, 2018.
- [18] Partially reduced sn/sno 2 porous hollow fiber: A highly selective, efficient and robust electrocatalyst towards carbon dioxide reduction. *Electrochimica Acta*, 285:70–77, 9 2018.
- [19] Fengwang Li, Lu Chen, Gregory P Knowles, Douglas R Macfarlane, and Jie Zhang. Hierarchical Mesoporous SnO 2 Nanosheets on Carbon Cloth : A Robust and Flexible Electrocatalyst for CO 2 Reduction with High Efficiency and Selectivity. pages 505–509, 2017.
- [20] Yanan Li, Jinli Qiao, Xia Zhang, Tao Lei, Abel Girma, and Yuyu Liu. Rational Design and Synthesis of SnO x Electrocatalysts with Coralline Structure for Highly Improved Aqueous CO 2 Reduction to Formate. pages 1618–1628, 2016.
- [21] Chenchen Zhao and Jianlong Wang. Electrochemical reduction of co2 to formate in aqueous solution using electro-deposited sn catalysts. *Chemical Engineering Journal*, 293:161–170, 06 2016.
- [22] Qinian Wang, Heng Dong, and Hongbing Yu. RSC Advances Fabrication of a novel tin gas di ff usion electrode for electrochemical reduction of carbon dioxide to formic acid †. pages 59970–59976, 2014.
- [23] Seunghwa Lee, Joey D Ocon, Young-il Son, and Jaeyoung Lee. Alkaline CO 2 Electrolysis toward Selective and Continuous HCOO Production over SnO 2 Nanocatalysts. 2015.
- [24] Sheng Zhang, Peng Kang, and Thomas J Meyer. Nanostructured Tin Catalysts for Selective Electrochemical Reduction of Carbon Dioxide to Formate. (c):3–6, 2014.
- [25] Song Yi Won D.H., Choi, Soon Kwan Jeong, Hak Joo Kim, Il-hyun Baek, and Ki Tae Park. Electrochemical Reduction of Carbon Dioxide to Formate on Tin Lead Alloys. 2016.

- [26] G K Surya Prakash, Federico A Viva, and George A Olah. Electrochemical reduction of CO<sub>2</sub> over Sn-Na<sub>2</sub>Fi on  $\text{O}_2$  coated electrode for a fuel-cell-like device. *Journal of Power Sources*, 223:68–73, 2013.
- [27] Bijandra Kumar, Veerendra Atla, J Patrick Brian, Sudesh Kumari, Tu Quang Nguyen, Mahendra Sunkara, and Joshua M Spurgeon. Reduced SnO<sub>2</sub> Porous Nanowires with a High Density of Grain Boundaries as Catalysts for Efficient Electrochemical CO<sub>2</sub>-into- HCOOH Conversion. pages 3645–3649, 2017.
- [28] Katarzyna Bejtka, Juqin Zeng, Adriano Sacco, Micaela Castellino, Simelys Herna, M Amin Farkhondehfar, Umberto Savino, Simone Ansaloni, Candido F Pirri, and Angelica Chiodoni. Chainlike Mesoporous SnO<sub>2</sub> as a Well-Performing Catalyst for Electrochemical CO<sub>2</sub> Reduction. 2019.
- [29] Karthikeyan Saravanan, Yasemin Basdogan, James Dean, and John A Keith. electroreduction on tin oxide and predictions of Ti, V, Nb and Zr dopants for improved catalysis †. pages 11756–11763, 2017.
- [30] Zhouguang Lu, Chris Lee, and Shanshan Zeng. Electrochemical fabrication and optical properties of porous tin oxide films with structural colors. (October), 2014.
- [31] Can Lu, Junxia Wang, Dawei Meng, Anqi Wang, Yongqian Wang, and Zhengxin Zhu. Tunable synthesis of nanoporous tin oxide structures on metallic tin by one-step electrochemical anodization. *Journal of Alloys and Compounds*, 685:670–679, 2016.
- [32] By Chris Van De Goor. Influence of temperature and pH on the hydrogen evolution reaction ( HER ) on platinum.
- [33] Leszek Zaraska, Karolina Gawlak, Magdalena Gurgul, Magdalena Dziurka, Marlena Nowak, Dominika Gilek, and Grzegorz D Sulka. Applied Surface Science Influence of anodizing conditions on generation of internal cracks in anodic porous tin oxide films grown in NaOH electrolyte. *Applied Surface Science*, 439:672–680, 2018.
- [34] By Heon-cheol Shin, Jian Dong, and Meilin Liu. Porous Tin Oxides Prepared Using an Anodic Oxidation Process \*\*. (3):237–240, 2004.
- [35] Leszek Zaraska, Dominika Gilek, Karolina Gawlak, Marian Jaskuła, and Grzegorz D Sulka. Applied Surface Science Formation of crack-free nanoporous tin oxide layers via simple one-step anodic oxidation in NaOH at low applied voltages. *Applied Surface Science*, 390:31–37, 2016.
- [36] Lei Ran, Danyang Zhao, Xueping Gao, and Longwei Yin. Highly crystalline Ti-doped SnO<sub>2</sub> hollow structured photocatalyst with enhanced

- photocatalytic activity for degradation of organic. pages 4225–4237, 2015.
- [37] Van Wijck. (12) United States Patent. 1(12), 2003.
- [38] Veeco | technologies & products | atomic layer deposition | ald overview. <https://www.veeco.com/technologies-and-products/atomic-layer-deposition/ald-overview>. (Accessed on 12/01/2019).
- [39] Markus Bosund, Emma M Salmi, and Risto Peltonen. Atomic layer deposition into ultra-high aspect ratio structures with a stop-flow ALD reactor. pages 2–3, 2016.
- [40] Jerzy Haber, Jochen H Block, and Bernard Delmon. 1230 3.3. pages 1230–1258, 1979.
- [41] Derek Shaw. *Diffusion in Semiconductors*, pages 1–1. Springer International Publishing, Cham, 2017.
- [42] Leszek Zaraska, Karolina Syrek, Katarzyna E Hnida, Aleksandra Krzysik, Ł Tomasz, Marian Jasku, and Grzegorz D Sulka. Electrochimica Acta Nanoporous tin oxides synthesized via electrochemical anodization in oxalic acid and their photoelectrochemical activity. 205:273–280, 2016.
- [43] Anna Palacios-padrós, Marco Altomare, Kiyoung Lee, and Ismael Díez-pørez. Controlled Thermal Annealing Tunes the Photoelectrochemical Properties of Nanochanneled Tin-Oxide Structures. pages 1133–1137, 2014.
- [44] Nicolas Brodusch. APPLIED SCIENCES AND TECHNOLOGY Field Emission Scanning Electron Microscopy New Perspectives for Materials Characterization.
- [45] Advanced Technology. A Guide to Scanning Microscope Observation A Guide to Scanning Microscope Observation.
- [46] Des McMorro Jens Als-Nielsen. *Elements of Modern X-ray Physics, Second Edition*.
- [47] Harald Ibach and Hans Liith. *Solid-state physics*.
- [48] Guixia Zhao, Xiangxue Wang, and Xiangke Wang. Progress in catalyst exploration for heterogeneous CO<sub>2</sub> reduction and utilization : a critical review. pages 21625–21649, 2017.
- [49] Ibram Ganesh. Electrochemical conversion of carbon dioxide into renewable fuel chemicals – The role of nanomaterials and the commercialization. 59:1269–1297, 2016.
- [50] Weixin Lv, Rui Zhang, Pengran Gao, and Lixu Lei. Studies on the faradaic efficiency for electrochemical reduction of carbon dioxide to formate on tin electrode. *Journal of Power Sources*, 253:276–281, 2014.

- [51] C. Korzeniewski. Chapter 6 - ir spectroelectrochemistry: Instrumentation and applications of external reflection, atr, and transmission sampling. In Shi-Gang Sun, Paul Andrew Christensen, and Andrzej Wieckowski, editors, *In-situ Spectroscopic Studies of Adsorption at the Electrode and Electrocatalysis*, pages 179 – 208. Elsevier Science B.V., Amsterdam, 2007.
- [52] Kelley J Rountree, Brian D Mccarthy, Eric S Rountree, Thomas T Eisenhart, and Jillian L Dempsey. A Practical Beginner ' s Guide to Cyclic Voltammetry. 2017.
- [53] Thomas Burdyny and Wilson A. Smith. CO 2 reduction on gas-diffusion electrodes and why catalytic performance must be assessed at commercially-relevant conditions. *Energy and Environmental Science*, 12(5):1442–1453, 2019.
- [54] Hydrogen Technology. Introduction to Hydrogen Technology. pages 1–51.
- [55] Rahman Daiyan, Xunyu Lu, Yun Hau Ng, and Rose Amal. Catalysis Science & Technology reduction of carbon dioxide to formate †. pages 2542–2550, 2017.
- [56] Chengzhen Chen, Bo Zhang, Juhua Zhong, and Zhenmin Cheng. Selective electrochemical CO 2 reduction over highly porous gold film. pages 7–10, 2017.
- [57] Hayder Hashim. chromatography and HPLC principles. (January), 2018.
- [58] Bishnu P. Regmi and Masoud Agah. Micro Gas Chromatography: An Overview of Critical Components and Their Integration. *Analytical Chemistry*, 90(22):13133–13150, 2018.
- [59] Rahman Md. Musfiquir, A.M. Abd El-Aty, Jeong-Heui Choi, Ho-Chul Shin, Sung Chul Shin, and Jae-Han Shim. Basic Overview on Gas Chromatography Columns. *Analytical Separation Science*, pages 823–834, 2015.
- [60] Aqua regia. 2(2):527200, 2014.
- [61] Marco Laurenti, Giancarlo Canavese, Adriano Sacco, Marco Fontana, Katarzyna Bejtka, Micaela Castellino, Candido Fabrizio Pirri, and Valentina Cauda. Nanobranched ZnO Structure : p-Type Doping Induces Piezoelectric Voltage Generation and Ferroelectric – Photovoltaic Effect. pages 4218–4223, 2015.
- [62] Deposition of Titanium Dioxide Coating on Plastic for Medical Purposes Lavinia Tjugito Submitted in Partial Fulfilment of the Requirements for the Degree of Master of Philosophy. (March), 2010.

- [63] Kiran Jain, R P Pant, and S T Lakshmikumar. Effect of Ni doping on thick film SnO<sub>2</sub> gas sensor. 113:823–829, 2006.